1   **Stimulation-responsive enhancers regulate inflammatory gene activation through**

2   **retention and modification of H2A.Z-variant accessible nucleosomes**

3

4   Audrey Sporrij[1,2], Meera Prasad[2]*, Brejnev Muhire[3,4]*, Eva M. Fast[1,2]*, Margot E.

5   Manning[1,2], Avik Choudhuri[1,2], Jodi D. Weiss[1,2], Michelle Koh[1,2], Song Yang[2], Robert E.

6   Kingston[3], Michael Y. Tolstorukov[5], Hans Clevers[6,7], Leonard I. Zon[1,2,8#]

7

8   [1] Harvard Department of Stem Cell and Regenerative Biology, Harvard

9   University, Cambridge, MA 02138, USA

10   [2] Stem Cell Program and Division of Hematology/Oncology, Boston

11   Children's Hospital, Boston, MA, USA

12   [3] Department of Molecular Biology, Massachusetts General Hospital and Harvard Medical

13   School, Boston, Massachusetts 02114, USA

14   [4] Present address: Center for Cancer and Cell Biology, Van Andel Research Institute,

15   Grand Rapids, MI 49503

16   [5] Department of Informatics and Analytics, Dana-Farber Cancer Institute, Boston, MA

17   02215

18   [6] Oncode Institute, Hubrecht Institute, Royal Netherlands Academy of Arts and

19   Sciences (KNAW) and University Medical Center (UMC) Utrecht, Utrecht, the

20   Netherlands

21   [7] Princess Máxima Center for Pediatric Oncology, Utrecht, the Netherlands

22   [8] Harvard Stem Cell Institute, Harvard Medical School and Howard Hughes Medical

23   Institute, Boston, MA, USA

24

25   [#] Correspondence to: Leonard I. Zon, leonard.zon@enders.tch.harvard.edu

26

27   * These authors contributed equally

28

Abstract

Prostaglandin E2 (PGE$_2$) and 16,16-dimethyl-PGE$_2$ (dmPGE$_2$) are important regulators of hematopoietic stem and progenitor cell (HSPC) fate and offer potential to enhance stem cell therapies[1,2]. The mechanism of gene regulation in response to dmPGE$_2$ is poorly understood. Here, we show that dmPGE$_2$ regulates inflammatory gene induction by modulating the chromatin architecture and activity of enhancer elements in human HSPCs. We identified the specific genomic reorganization at stimuli-responsive enhancers that permits rapid transcriptional activation. We found that dmPGE$_2$-inducible enhancers retain MNase-accessible, H2A.Z-variant nucleosomes that are permissive to binding of the transcription factor CREB. CREB binding to enhancer nucleosomes is concomitant with deposition of the histone acetyltransferases p300 and Tip60 on chromatin. Subsequent H2A.Z acetylation improves chromatin accessibility at stimuli-responsive enhancers. Our findings support a model where histone variant nucleosomes retained within inducible enhancers facilitate transcription factor (TF) binding. Acetylation of histone variant nucleosomes by TF-associated nucleosome remodelers creates the accessible nucleosome landscape required for immediate enhancer activation and gene induction. Our work provides a mechanism by which inflammatory mediators such as dmPGE$_2$ lead to acute transcriptional changes and alter HSPC behavior.

Introduction

Hematopoietic stem cells are characterized by their unique ability to self-renew and differentiate into all mature blood cell lineages. During normal homeostasis and in conditions of stress such as injury or inflammation, HSPCs maintain an appropriate balance of the hematopoietic system. HSPCs sense and respond to a variety of extrinsic signals that regulate their quiescence, proliferation, and differentiation[3,4]. A main mechanism of adaptation involves the activation of TFs that are downstream of signal transduction pathways to ensure appropriate transcriptional responses upon

2

60 stimulation[5,6]. In higher eukaryotes, gene expression is regulated by the coordinated

61 action of enhancers and promoters[7]. Stimuli-responsive TFs (STFs) tend to operate within

62 the *cis*-regulatory repertoire that is established during cell fate specification and

63 maintained by constitutive binding of lineage specific master TFs (MTFs)[8]. The access of

64 STFs to these regulatory elements and their interaction with cofactors, such as

65 transcriptional activators and chromatin remodeling complexes, depends largely on the

66 local chromatin architecture[9]. Generally accepted features of active regulatory regions

67 include open chromatin conformation, histone modifications and TF binding[10]. While

68 promoters consist of a nucleosome depleted region that is established by chromatin

69 remodelers, general TFs, and the basal transcription machinery, the typical chromatin

70 organization and nucleosome configuration at enhancers remains unclear[11].

71 Prostaglandins are physiologically active lipids produced in response to mechanical,

72 chemical, or immunological stimuli. They sustain a variety of homeostatic and pathogenic

73 functions. This includes roles in the inflammatory response. PGE_2 is one of the most

74 abundant prostaglandins produced in the body[12]. PGE_2 and its stable derivative $dmPGE_2$

75 act as important regulators of vertebrate HSPC development and homeostasis[1,13]. *Ex vivo*

76 pulse exposure of HSPCs to $dmPGE_2$ enhances engraftment and self-renewal in mice

77 and clinical studies indicate benefits for hematopoietic stem cell transplantation (HSCT)

78 outcomes in humans[2,14]. $dmPGE_2$ predominantly exerts its effects by binding to the PGE_2

79 receptor (EP) subtypes EP2 and EP4 on HSPCs[15]. Interaction with these G-coupled

80 protein receptors enhances intracellular cAMP levels which activates signaling cascades

81 and downstream effectors, for instance Wnt and β-Catenin[13]. Improved engraftment

82 presumably results from upregulation of genes implicated in HSPC homing, such as

83 *CXCR4*[16]. As enhancement of HSPC function by external stimuli supports a strategy to

84 improve HSCTs, understanding the mechanism of gene regulation in response to

85 inductive signals can provide a significant clinical opportunity.

86 Here, we sought to address how transcriptional induction is regulated during the HSPC

87 response to $dmPGE_2$. We exploited inducible TF binding to chromatin and identified, and

88 then mechanistically dissected, enhancers controlling inflammatory gene expression

89 changes in HSPCs. We assessed the chromatin accessibility and nucleosome

90 organization of regulatory regions responsive to $dmPGE_2$ and studied how the higher

91   order chromatin structures changed following induction. We found that stimuli-induced
92   enhancers retained MNase-accessible nucleosomes. These enhancer nucleosomes
93   were enriched with the non-canonical histone variant H2A.Z and remodeled but not
94   evicted during acute stimulation. Rather than prohibiting TF binding, we observed
95   enrichment of the $dmPGE_2$ responsive TF CREB at accessible nucleosomes within
96   inducible enhancers. CREB binding is concomitant with deposition of the chromatin
97   remodelers p300 and Tip60 that acetylates histone variant H2A.Z following $dmPGE_2$
98   stimulation. This may further improve nucleosomes accessibility at stimuli-responsive
99   enhancers and allow for binding of additional TFs and co-activator complexes. We
100   suggest the nucleosome organization at enhancers is not exclusively repressive to gene
101   regulation but favors STF binding, which enables rapid enhancer activation and
102   inflammatory gene induction.

103

104   **Results**

105

106   *CREB regulates gene expression changes through binding at enhancer elements*

107

108   We sought to define the molecular mechanisms that underlie the transcriptional response
109   of HSPCs to $dmPGE_2$. We exposed human mobilized peripheral blood CD34$^+$ HSPCs to
110   10μM $dmPGE_2$ for 2 hours and performed extensive gene expression and chromatin
111   profiling (Figure 1A). Using RNA-sequencing (RNA-Seq), we identified a total of 687
112   consistent differentially expressed genes (DEGs) after 2 hours of $dmPGE_2$ treatment,
113   when compared to vehicle (DMSO) treated control cells (Figure 1B). The effect of
114   $dmPGE_2$ on gene expression was overwhelmingly stimulatory. More specifically, 535
115   genes were ≥ 1.5-fold upregulated. This includes a significant number of genes involved
116   in cell migration and cell cycle regulation (Supplemental Figure 1A, 1C). Among the
117   upregulated set were genes representative of $dmPGE_2$/cAMP/PKA signaling, including
118   *PDE4B* and *PTGS2*[17]; several chemokines and cytokines, such as *CXCL2* and *CXCL8*[18];
119   and genes known to restrict HSPC proliferation and differentiation, for instance *NR4A1*
120   and *JUNB*[19,20](Figure 1C, Supplementary Table 1). We validated the gene expression
121   signature observed by RNA-Seq through RT-qPCR in HSPCs for representative genes

122 (Supplemental Figure 1D). 152 genes showed a $\leq$ 0.67-fold decrease in expression

123 (Supplemental Figure 1B, Supplementary Table 1). Among the repressed genes, we

124 found enrichment of genes that regulate cell division, such as *HOXB4* and *CCNF*[21]. To

125 evaluate the functional impact of gene expression changes in human HSPCs, we

126 assessed cell migration after dmPGE$_2$ treatment *in vitro.* By transwell migration assay,

127 which served as a proxy for the previously observed engraftment phenotype[1], we

128 observed greater migration of HSPCs after exposure to dmPGE$_2$ (Supplemental Figure

129 1E). These data showed that enhanced engraftment *in vivo* after dmPGE$_2$ stimulation is,

130 in part, driven by transcriptional induction of migration genes.

131 The TF CREB has previously been associated with dmPGE$_2$ signaling[22]. Indeed, our

132 transcriptomic analysis revealed that 30% (158/535) of upregulated genes are known

133 targets of CREB (Supplemental Figure 2A). CREB binds to cyclic-AMP response

134 elements (CREs) near its target genes where it, upon phosphorylation at serine 133

135 (S133) by protein kinases, promotes the recruitment of co-activator proteins[23]. This

136 increases transcription of CREB-dependent genes[24]. One of protein kinases that

137 phosphorylates CREB at S133 is protein kinase A (PKA). We assessed S133

138 phosphorylation of CREB in HSPCs after dmPGE$_2$ treatment. Western blot analysis

139 revealed increased abundance of S133 phosphorylated CREB (pCREB) while total TF

140 protein levels remain unaltered (Supplemental Figure 2B). To correlate pCREB with gene

141 induction, we performed chromatin immunoprecipitation sequencing (ChIP-Seq) with an

142 antibody against pCREB. We found 31,198 binding sites (FDR < 0.1%) in CD34$^+$ HSPCs

143 treated for 2 hours with dmPGE$_2$ compared to 8,332 sites in DMSO (Supplemental Figure

144 2C, Supplementary Table 2). Correlation of pCREB occupancy to DEGs showed

145 enrichment of pCREB at genes induced by dmPGE$_2$ (Figure 1D). In fact, 79% of the

146 upregulated genes contained at least one pCREB peak in the proximity, that is a window

147 from -5kb upstream of the transcription start site (TSS) to +5kb downstream of the TTS,

148 after dmPGE$_2$ stimulation compared to 47% prior to treatment (Figure 1D). This value

149 increased to 85% by extending the window up to -100kb from the TSS to +25kb from TTS

150 (Supplemental Figure 2C). Besides a higher percentage of upregulated genes containing

151 pCREB, the TF density was also >2 times higher at upregulated genes compared to

152 noninduced genes (Figure 1E, Supplemental Figure 1D). We observed no clear

153   correlation between the magnitude of the transcriptional response and the density of
154   pCREB (Supplemental Figure 1F). Genes downregulated by dmPGE$_2$ showed no
155   additional enrichment in pCREB compared to noninduced genes. This data demonstrated
156   that dmPGE$_2$ regulates pCREB activity and genomic binding near transcriptionally
157   induced genes.
158   We next assessed the genomic location of pCREB bound regions. 23,386 (75%) sites
159   displayed unique pCREB enrichment ('inducible' pCREB regions) in dmPGE$_2$ treated
160   HSPCs compared to control treated cells. The other 7,812 (25%) pCREB sites were
161   present in both control and stimulated HSPCs ('ubiquitous' pCREB regions). The majority
162   of inducible pCREB sites were located distal to the TSS of genes, with a strong
163   representation in intronic and intergenic sequences (Figure 1F, 1G). Ubiquitous pCREB
164   sites were predominantly enriched in promoter regions. This indicated that pCREB
165   binding at putative distal regulatory elements plays a pivotal role in upregulating dmPGE$_2$
166   response genes.
167
168   *Inducible enhancers gain master and signaling transcription factor binding*
169
170   To understand the epigenetic impact of dmPGE$_2$ on distal regulatory elements, we
171   determined the effects of a 2-hour stimulation on the state of enhancers in HSPCs.
172   H3K27ac distinguishes active enhancers from primed and poised enhancer elements that
173   are marked by H3K4me1 alone or with H3K27me3, respectively[25]. We performed
174   chromatin immunoprecipitation sequencing (ChIP-Seq) for these classifying histone
175   modifications. We assessed H3K27ac enrichment in control and dmPGE$_2$ stimulated
176   HSPCs and identified a total of 25,998 active distal regulatory elements (Supplementary
177   Table 3). Enhancers that regulate stimulus responsive gene programs can be
178   distinguished from other active enhancers by their specific increase in H3K27ac upon
179   receipt of the stimulus[26-28]. Comparison of H3K27ac enrichment between control and
180   dmPGE$_2$ treated HSPCs allowed us to identify putative distal enhancers involved in the
181   response to dmPGE$_2$. We identified a total of 954 (3.7%) enhancers that gained significant
182   enrichment in H3K27ac following dmPGE$_2$ treatment (Supplemental Figure 3A-B, and
183   Methods). A subset of these stimuli-inducible enhancers (498/954, 52%) were only

6

184   detected as active regulatory regions after $dmPGE_2$ stimulation. While these 'de novo'

185   enhancers were depleted of H3K27ac prior to stimulation, their

186    $H3K4me1^{high}$/$H3K27me3^{low}$ state indicated that de novo enhancers reside in a primed

187   state prior to activation (Figure 2A-B). The other fraction of $dmPGE_2$-inducible enhancers

188   (456/954, 48%) displayed significant enhancement in H3K27ac enrichment after $dmPGE_2$

189   treatment ('enhanced', Figure 2A, Supplemental Figure 3C). Since the number of

190   noninducible enhancers (25,044 regions, 96.3%) is much larger than the set of inducible

191   enhancers, we randomly sampled a comparable number of noninducible enhancers

192   ('background', 486) to ensure that observed differences are not due to variations in the

193   size of defined enhancer categories. To assess epigenetic transitions at inducible

194   enhancers, we profiled genome accessibility by assay for transposase-accessible

195   chromatin sequencing (ATAC-Seq). We found a profound increase in DNA accessibility

196   at inducible enhancers compared to background enhancers after $dmPGE_2$ stimulation

197   (Figure 2A-B), which is a sign of active chromatin reorganization[29]. In addition, the mean

198   ATAC-Seq signal prior to activation of de novo enhancers suggested preexisting, yet

199   minimal, accessibility before stimulation. This revealed that $dmPGE_2$ stimulation results

200   in rapid activation of stimuli-responsive enhancers that is concomitant with increased

201   chromatin accessibility.

202   It is well known that TFs act as anchors to recruit chromatin remodelers to regulate gene

203   expression[7]. Most STFs do not possess pioneering activity and therefore preferentially

204   bind DNA elements located within nucleosome depleted regions. Moreover, STFs often

205   land at regulatory elements predefined by lineage specific MTF that have pioneer

206   functions[27,30]. Given these insights, we assessed both pCREB occupancy and binding of

207   the HSPC MTFs GATA2 and PU.1 at enhancers prior to and after $dmPGE_2$ treatment.

208   We found that pCREB colocalized with GATA2 and PU.1 at stimuli-responsive enhancers

209   (Figure 2A, 2C). We moreover observed that inducible enhancers not only gain pCREB

210   but also GATA2 and PU.1 enrichment after $dmPGE_2$ stimulation (Figure 2B-C). No

211   enrichment in MTF occupancy was observed in background enhancers (Figure 2A-B,

212   Supplemental Figure 3E). These data showed that $dmPGE_2$-inducible enhancers gain

213   both STF and additional MTF deposition following stimulation.

214 The contribution of distal regulatory regions for transcriptional activation of dmPGE$_2$ target

215 genes is illustrated by the changes in the expression of genes regulated by stimuli-

216 responsive enhancers compared to those regulated by background enhancers (Figure

217 3A, Supplemental Figure 4A). We tentatively assigned enhancers to individual nearest

218 genes. To reasonably limit arbitrariness in gene assignment, we only considered genes

219 with a mapped TSS within 15kb of an enhancer. The genes nearest to stimuli-inducible

220 enhancers showed a greater transcriptional response than genes annotated to

221 background enhancers (Figure 3A, Supplemental Figure 4A). This indicates that

222 differential enhancer activity is directly reflected in gene expression levels. Importantly,

223 genes associated with inducible enhancers belonged to several pathways, including cell

224 signaling and blood cell migration such as *SGK1, CALCRL, CXCL2, CXCL5,* and *ITGA4*

225 (Figure 2C, Supplementary Table 4). We found a clear correlation between the number

226 of genes showing differential expression and the changes in enhancer activity. 16% of

227 genes nearest to de novo enhancers display $\geq$ 1.5-fold induction after dmPGE$_2$ treatment,

228 compared to 9% of enhanced and 3% of background enhancers (Figure 3B,

229 Supplemental Figure 4B). In total, 83 (16%) of the 535 upregulated genes were regulated

230 by at least one stimuli-responsive enhancer (Figure 3C, Supplemental Figure 4C). This

231 demonstrated that dmPGE$_2$-mediated activation of stimuli-responsive enhancers

232 correlates with modulation of gene expression.

233 To gain a better understanding of the role of pCREB at inducible enhancers, we further

234 segmented enhancers based on the presence or absence of pCREB after dmPGE$_2$

235 treatment. We found that 208/498 (42%) de novo, 210/456 (46%) enhanced and 125/486

236 (26%) background enhancers to contain at least 1 pCREB ChIP-Seq peak after dmPGE$_2$

237 treatment. Chromatin accessibility and MTF binding increased more profoundly, but not

238 exclusively, at pCREB$^+$ stimuli-inducible enhancers (Figure 3D). The results support a

239 prominent, but not restricted, role for pCREB in regulating gene expression through

240 binding at inducible enhancers. Additionally, pCREB$^+$ stimuli-responsive enhancer

241 showed greater transcriptional changes than those without pCREB (Figure 3E,

242 Supplemental Figure 4D). Together, our data suggested that increased enhancer

243 chromatin accessibility and the cooperative binding MTFs and STFs at stimuli-responsive

244 regulatory regions drives transcriptional induction.

245

Inducible enhancers retain accessible nucleosomes after inflammatory stimulation

247

Various studies showed that TFs preferentially bind to sites of open, accessible chromatin[31]. However, recent work indicated that accessible chromatin may not necessarily represent nucleosome depleted regions[32,33]. To test whether greater chromatin accessibility at stimuli-responsive enhancers is due to nucleosome depletion, we performed micrococcal nuclease sequencing (MNase-Seq). This allowed us to map nucleosome positions and nucleosome occupancy changes after dmPGE$_2$ stimulation. Because nucleosomes have varying sensitivities to enzymatic digestion, MNase titrations were performed to obtain a comprehensive map of the nucleosome landscape within a genome[32-34]. While comparing occupancy profiles between individual titration points provides insights on nucleosomal accessibility, the combinatorial analysis of all titration points within a given condition generates a complete view of the nucleosome organization[32] (Supplemental Figure 5A). We prepared native nuclei from HSPCs treated with either DMSO and dmPGE$_2$ and exposed them to increasing units of MNase. We selected 4 digestion points that generated increasingly larger fractions of mononucleosomal-size DNA. Mononucleosomal fractions comprised around 10%, 25%, 50%, and 75% of the input chromatin, respectively (Supplemental Figure 5B). Individual MNase titration profiles within a condition, as well as pooled average nucleosome occupancy profiles, revealed a TSS pattern similar to those previously reported[32] (Supplemental Figure 5C-D). We observed lower average nucleosome occupancy at TSS-proximal regions of dmPGE$_2$-responsive genes after treatment (Supplemental Figure 5E). This inverse correlation aligns with former studies which identified high levels of transcription to be concomitant with nucleosome eviction at the TSS, as elongation by RNA Polymerase II is thought to disrupt the nucleosomal organization[35,36].

When assessing the nucleosome organization at inducible enhancers, we found that these regions presented in high nucleosome occupancy states when compared to active promoters (Figure 4A, Supplemental Figure 5E). Although high occupancy regions are traditionally thought of as 'closed', recent work indicated that accessible regulatory regions can retain nucleosomes[33,34]. We determined whether nucleosomes were

276   repositioned or evicted at $dmPGE_2$-responsive enhancers following stimulation. No

277   decrease in average nucleosome occupancy was observed at stimuli-responsive

278   enhancers. Inducible enhancers demonstrated higher nucleosome occupancy after

279      $dmPGE_2$ treatment (Figure 4A). This was not observed at background enhancers,

280   indicating specificity of the phenomena to $dmPGE_2$-inducible enhancers. Our data

281   suggests that stimuli-responsive enhancers retained nucleosomes upon activation, rather

282   than remodeled to a nucleosome free organization via nucleosome eviction.

283   Nucleosomes profiles from individual MNase titration points can be leveraged to

284   determine how MNase sensitivity changes in specific regions (Supplemental Figure 5A).

285   Light MNase conditions preferentially release accessible and unstable nucleosomes

286   whereas stable nucleosomes are more resistant to enzyme digestion and only released

287   at higher MNase concentrations[32-34]. We found greater low MNase-Seq signal at inducible

288   enhancers after $dmPGE_2$ stimulation (Figure 4B, upper panel) whereas high MNase

289   digestion degraded the nucleosomal DNA fragments (Figure 4B, bottom panel). No

290   changes in low MNase sensitivity were observed in background enhancers. Greater low

291   MNase sensitivity after $dmPGE_2$ treatment indicates a higher presence of MNase

292   accessible nucleosomes. This shows that nucleosomes retained within inducible

293   enhancers gained low MNase sensitivity of upon stimulation.

294   To ensure that the low MNase-Seq signal represents nucleosomes, we performed ChIP-

295   Seq for the core histones H2B and H4 (Figure 4C, Supplemental Figure 6A). Inducible

296   enhancers were not depleted of core histones prior to or after $dmPGE_2$ stimulation. This

297   is in line with our MNase-Seq data and suggested that nucleosomes are indeed present,

298   and retained at, $dmPGE_2$-responsive enhancers. In contrast to our expectations that

299   increased chromatin accessibility at inducible enhancers (Figure 2B) resulted from

300   nucleosome displacement or eviction, our MNase-Seq and ChIP-Seq data revealed that

301   stimuli-responsive enhancers retained accessible nucleosomes upon activation.

302   Based on the accessible nucleosomes at enhancers, we next evaluated the relationships

303   between nucleosomes and binding of pCREB at inducible enhancers. 10,169/23,386

304   (43%) of pCREB binding sites uniquely present after $dmPGE_2$ treatment are located

305   within the 25,998 active enhancers identified in HSPCs. We observed enrichment of

306   phased nucleosomes at the summit of $dmPGE_2$-unique pCREB peaks located within

307   enhancers, both before and after dmPGE$_2$ treatment (Figure 5A). To exclude the

308   possibility that the MNase-Seq fragments observed at pCREB sites within enhancers

309   represent non-histone proteins protecting from MNase digestion, we assessed fragment

310   size distribution (Supplemental Figure 6B). We found a fragment periodicity that is

311   characteristic for MNase-digested nucleosomes[37,38]. The majority of the MNase-Seq

312   fragments that coincide with pCREB binding was 148 base pairs (bp) in length. This

313   corresponds to precisely trimmed nucleosome core particles. Subnucleosomal peaks

314   showed a clear ~10bp periodicity that reflects the accessibility of DNA as it is wound along

315   the surface of the histone octamer[39]. This analysis suggested that MNase-Seq fragments

316   mapping to pCREB sites within enhancers represent nucleosomes. Looking specifically

317   at pCREB$^+$ stimuli-responsive enhancers, we observed that the effects of dmPGE$_2$ on

318   nucleosome occupancy and low MNase sensitivity described earlier are further amplified

319   at pCREB$^+$ regions (Figure 5B-C). Assessment of individual loci confirmed pCREB

320   binding at stimuli-responsive enhancers that show greater low MNase signal and

321   increased nucleosome occupancies after dmPGE$_2$ treatment (Figure 4C). Together, the

322   data demonstrated that accessible nucleosomes are retained at dmPGE$_2$-responsive

323   enhancers and that these nucleosomes are not prohibitive of pCREB binding.

324

325   *Modification of H2A.Z-variant accessible nucleosomes at stimuli-responsive enhancers*

326

327   We hypothesized that nucleosome at enhancers may exert important roles in pCREB

328   binding. Nucleosome-driven TF binding has been observed for several other stress-

329   responsive TFs[40]. To understand the conformational changes that underlie increased low

330   MNase sensitivity of enhancer nucleosomes after dmPGE$_2$ stimulation, we investigated

331   other mechanisms that influence accessibility to nucleosomal DNA. Weakening of

332   internucleosomal interactions by covalent modifications of histones as well as the

333   introduction of histone variants increases DNA accessibility[41]. The histone variants H2A.Z

334   and H3.3 can be incorporated in replication independent manners and are associated

335   with enhancers[42-44]. Once incorporated, these non-canonical histones make for

336   destabilized 'fragile' nucleosomes[45]. We assessed histone variant abundance at

337   regulatory regions in the presence and absence of dmPGE$_2$ stimulation through ChIP-

338   Seq analysis for H2A.Z and H3.3. We observed a positive correlation between histone

339   variant deposition and enhancer activity, with more profound presence of H2A.Z and H3.3

340   at higher H3K27ac levels (Supplemental Figure 7C-E). The histone variants were also

341   found to occupy slightly different sites within enhancers. H2A.Z localized more central to

342   enhancers the region where TFs bind, whereas H3.3-variant nucleosomes followed a

343   more dispersed pattern and localized to the flanks of enhancers in a profile similar to

344   H3K27ac (Supplemental Figure 7C-E). We noted minimal changes in H2A.Z enrichment

345   following dmPGE$_2$ stimulation. We did observe incorporation of the histone variant H3.3

346   in the nucleosomes of enhancers (Supplemental Figure 7C-E). When specifically

347   assessing histone variants at pCREB[+] stimuli-responsive enhancers, we found that

348   pCREB binding directly overlaps with H2A.Z-variant nucleosomes (Figure 6A,

349   Supplemental Figure 7A). To confirm interaction of pCREB with H2A.Z-variant

350   nucleosomes, we performed complex immunoprecipitation (Co-IP) for pCREB and found

351   association between the TF and H2A.Z histones (Figure 6B, Supplemental Figure 7B).

352   These results indicated that pCREB overlaps with H2A.Z and suggest that DNA binding

353   of the TF is not prohibited by H2A.Z-variant nucleosomes.

354   H2A.Z is associated with both gene repression and activation[46]. This dual function is

355   attributed to post-translational regulation of the histone variant. Different H2A.Z histone

356   tail modifications recruit distinct interactors that mediate varying transcriptional outputs.

357   H2A.Z acetylation is associated with active transcription and dynamically regulated in

358   response to environmental signals[47,48]. Acetylation of H2A.Z occurs at active regulatory

359   regions where it promotes nucleosomes destabilization and an open chromatin

360   conformation. The histone acetyltransferases (HATs) p300 and Tip60 that acetylate

361   H2A.Z are known interactors of pCREB[49,50]. Both chromatin remodelers hold important

362   roles in hematopoietic stem cell fate[45,51-53]. Whereas Tip60 alone is not sufficient to

363   acetylate H2A.Z, p300 can rapidly and effectively acetylate H2A.Z-containing

364   nucleosomes on its own[54]. Hence, we assessed if acetylation of H2A.Z-variant

365   nucleosomes at stimuli-responsive enhancers underlies increased MNase sensitivity and

366   nucleosome accessibility after dmPGE$_2$ treatment. We found specific H2A.Zac

367   enrichment at stimuli-inducible enhancers whereas this was not observed in background

368   enhancers (Figure 6C-D, Supplemental Figure 7D). We furthermore noted that dmPGE$_2$

369   increased the abundance of both p300 and Tip60 at enhancers (Figure 6C-D,

370   Supplemental Figure 7D). pCREB interacts with a variety of chromatin remodelers,

371   including p300 and Tip60[49,54]. Binding patterns of two HATs at enhancers were highly

372   similar to pCREB after dmPGE$_2$ treatment (Figure 2B, Supplemental Figure 7D) and are

373   suggestive of complex interaction at enhancers. Together, our data revealed that pCREB

374   binds to H2A.Z-variant nucleosomes within enhancers following dmPGE$_2$ stimulation.

375   pCREB binding at stimuli-responsive enhancers is accompanied by nucleosome

376   remodeling through H2A.Z acetylation, likely mediated through interaction of CREB with

377   p300 and Tip60. H2A.Z acetylation at enhancers may underlie increased enhancer

378   accessibility, allowing additional chromatin factors to engage and ultimately drive acute

379   gene expression changes.

380

381   **Discussion**

382

383   Prostaglandin E2 is an important regulator of HSPC homeostasis. The distinct molecular

384   mechanisms through which PGE$_2$ and its stable derivative dmPGE$_2$ affect HSC function

385   are critical to understand yet remain elusive. Here, we find that the TF CREB is a key

386   player in the acute transcriptional response to dmPGE$_2$ by binding to, and activating, distal

387   regulatory elements. Specifically, we find that pCREB binds to H2A.Z-variant

388   nucleosomes that are retained within stimuli-induced, active enhancers and is

389   concomitant with acetylation of these histones. H2A.Z acetylation of enhancer

390   nucleosomes increases local chromatin accessibility, which in turn may help to recruit

391   and/or stabilize other HSPC specific TFs such as GATA2 to stimulate gene transcription.

392

393   CREB is a ubiquitously expressed nuclear, basic leucine zipper (bZIP) TF that regulates

394   over 5,000 genes in the mammalian genome. This includes genes controlling

395   proliferation, differentiation, and cell survival[55]. The TF is activated by a wide variety of

396   environmental stimuli and is an important regulator of cellular responses to stress. Most

397   studies focused on promoter-proximal effects of CREB binding. We showed that inducible

398   gene expression is characterized by binding of pCREB at TSS-distal enhancers regions.

399   Regulation of transcriptional responses through binding of CREB at enhancers has also

400   been observed in pancreatic beta cells[56]. Our data suggests that CREB employs distinct

401   mechanisms to regulate steady state versus inducible gene expression.

402

403   Genome wide assessment of the epigenetic landscape revealed that $dmPGE_2$ works

404   within the predetermined enhancer repertoire of HSPCs. $dmPGE_2$ stimulation activates a

405   set of pre-existing H3K4me1$^+$ enhancers through chromatin reorganization. $dmPGE_2$-

406   responsive enhancers rapidly gain accessibility and TF binding. Our work complements

407   the studies that showed that STFs localize to binding sites adjacent to master

408   regulators[30,57]. Although we did not identify the surfacing of latent enhancers, *i.e.* genomic

409   regulatory elements devoid of TFs and enhancer marks in unstimulated cells[27], a 2-hour

410   pulse of $dmPGE_2$ may be too short to allow for partial reprogramming of the available cis-

411   regulatory landscape. Latent enhancer activation may also be more associated with

412   differentiated cells rather than stem and progenitor populations[27].

413

414   We found stimuli-driven enrichment of the HSPC specific MTFs GATA2 and PU.1 at

415   inducible enhancers, especially those that gained pCREB binding after 2 hours of

416   treatment. Cofactor driven binding is common among non-pioneer TFs. It was only

417   recently implied that interaction between TFs can enhance pioneer factor binding at

418   previously sampled target sites[58-60]. Many studies have described the vital role of GATA2

419   in establishing the regulatory landscape for STFs in HSPCs[30,61]. GATA2 facilitates

420   enhancer-promoter loop formation[62], yet few have proposed signaling factors to play a

421   role in GATA2 binding and recruitment to chromatin. We suggest that GATA2 occupancy

422   may be directed and stabilized through cooperativity with STFs at stimuli-responsive

423   enhancers. Our work supports a model where pioneer factor occupancy at specific

424   subsets of enhancers is partially determined by engagement with signaling specific

425   cofactors.

426

427   An open chromatin structure surrounding TF binding sites constitutes a prerequisite for

428   transcriptional regulation. Our results show that inducible enhancers rapidly gain

429   accessibility and affinity for STFs and MTFs. While open chromatin regions are presumed

430   nucleosome depleted regions, we find that $dmPGE_2$-responsive enhancers exhibit a high

431 nucleosome occupancy both prior to and after stimulation of HSPCs. Moreover, retained
432 enhancer nucleosomes are not prohibitive of STF binding. pCREB occupancy at
433 enhancers overlaps with well-positioned nucleosomes, suggesting that pCREB can
434 initiate chromatin engagement and access binding sites organized within a positioned
435 nucleosome. Our work indicates that accessible nucleosomes at enhancers may facilitate
436 cooperativity between STFs and MTFs to ensure rapid transcriptional induction. Retention
437 of MNase accessible nucleosomes at regulatory elements was proposed to play a crucial
438 role in hormone signaling and tissue specific gene activation[33,40]. Retained nucleosomes
439 likely stabilize the interaction of TFs with DNA by facilitating interactions between TF-
440 associated factors, such chromatin remodeling complexes and histone tails[40].

441

442 Except for pioneer factors, most TFs are thought to be unable to bind nucleosomal DNA.
443 Although CREB is not traditionally described as a pioneer factor, novel studies revealed
444 the ability of CREB to open chromatin[63]. CREB was identified as a TF that displays an
445 orientated, asymmetric, binding preference near the dyad axis of the nucleosome when
446 engaging nucleosomal DNA[64,65]. We hypothesize that MNase accessible nucleosomes
447 within stimuli-responsive enhancers enable cooperative TF binding for rapid gene
448 activation.

449

450 Nucleosomes retained within stimuli-inducible enhancers were epigenetically pre-marked
451 by the histone variant H2A.Z. Although the precise function of H2A.Z at enhancers at
452 remains unclear, H2A.Z is an important regulator of enhancer activity in response to
453 stimuli. H2A.Z-rich enhancers display higher chromatin accessibility and gene induction
454 by promoting RNA polymerase II recruitment[42,46,66]. In contrast to hormone stimulation,
455 which was found to increase H2A.Z incorporation at enhancer nucleosomes[67], we found
456 limited changes in H2A.Z distribution after $dmPGE_2$ treatment. Instead, we noted that
457 H2A.Z-variant nucleosomes undergo histone tail acetylation following $dmPGE_2$
458 stimulation. Acetylated forms of H2A.Z are associated with an open chromatin
459 conformation and directly regulate transcription of enhancer RNAs[68-70]. Our work implies
460 that $dmPGE_2$-inducible H2A.Z acetylation underlies increased low MNase sensitivity and
461 enhanced nucleosomes accessibility at stimuli-responsive enhancers following $dmPGE_2$

462   treatment. We found that changes in post-translational acetylation of H2A.Z at stimuli-
463   responsive enhancers correlate with gene expression changes, indicating that H2A.Zac
464   is a prerequisite for appropriate transcriptional induction following dmPGE$_2$ stimulation.
465

466   Labile, H2A.Z-marked nucleosomes do not present an obstacle for pCREB binding, but
467   may facilitate TF binding and enhancer activity. We suggest that a critical feature of
468   pCREB is the recruitment of remodelers that opens the local nucleosome structure
469   through H2A.Z acetylation in enhancers. pCREB interacts with a variety of chromatin
470   remodelers. This includes the HATs p300 and Tip60, both known to interact with H2A.Z
471   and catalyze its acetylation[49,54,71]. The recruitment of p300 to chromatin in a stimulus-
472   dependent manner observed here is consistent with interactions between chromatin
473   remodelers and other STFs[72-74]. Localization of p300 is concomitant to pCREB binding,
474   suggesting pCREB-p300 complex formation at enhancers upon dmPGE$_2$ stimulation.
475   pCREB facilitated recruitment of Tip60 to enhancers complements previously described
476   observations of Tip60 binding to a subset of enhancers and acetylating H2A.Z to promote
477   expression of HSC genes[71,75]. The acetylation of H2A.Z-variant enhancer nucleosomes
478   may create a chromatin environment permissive of enhancer activity and transcription.
479

480   In conclusion, this study reveals how specific genomic reorganization at a stimuli-
481   responsive group of enhancers is directly translated into regulatory element activation
482   and transcriptional induction. Our findings support a model where STFs and MTFs
483   cooperate with nucleosomes to regulate activity of cis-regulatory elements that mediate
484   adequate responses to environment signals. While the combination of cooperative
485   lineage-specific MTF and inducible STF binding provides context and responsiveness to
486   external stimuli, histone variant nucleosomes retained within inducible enhancers may
487   facilitate TF binding by stabilizing chromatin complexes. Subsequent acetylation of
488   histone variant nucleosomes by TF-associated nucleosome remodelers creates the
489   accessible nucleosome landscape required at active transcriptional enhancers to ensure
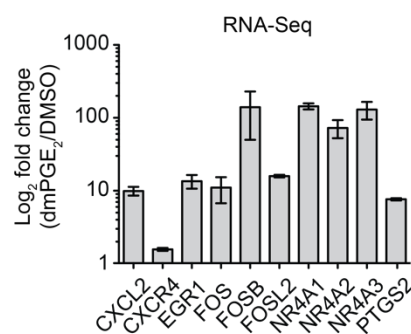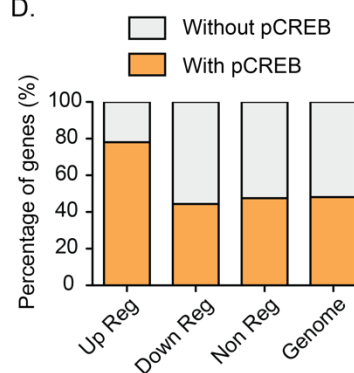490   strong gene activation.
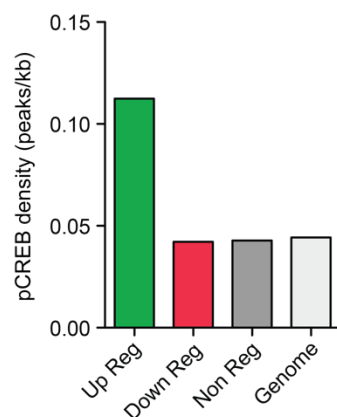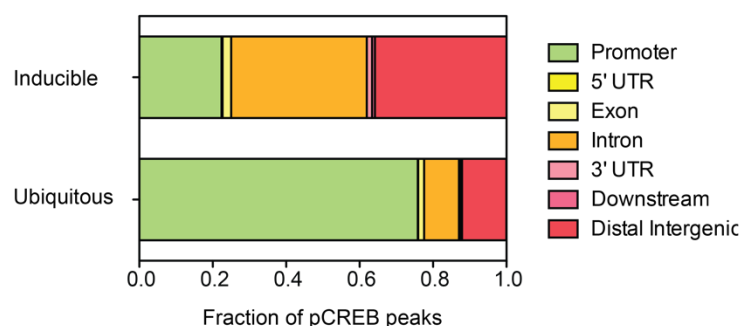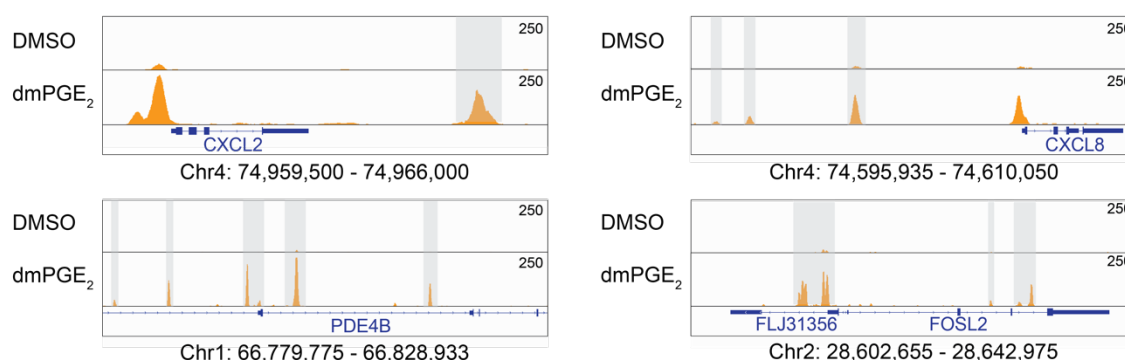491

492 **Figure 1.**

493
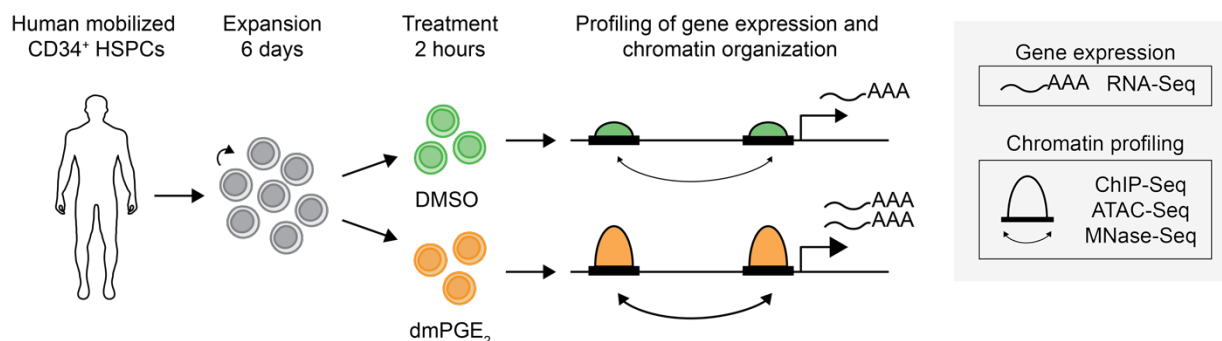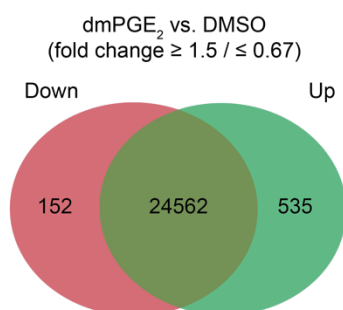
494 **Figure 1. phospho-CREB regulates dmPGE$_2$-induced gene expression changes**
495 **through binding at distal regulatory elements.** (A) Schematic representation of the
496 experimental approach used in this study. Cells are stimulated for 2 hours with dmPGE$_2$
497 or vehicle control (DMSO) after which transcriptome and epigenome profiling was
498 performed. (B) Venn diagram showing the number of genes upregulated in green (535)
499 and downregulated in red (152) in CD34$^+$ HSPCs after 2 hours of dmPGE$_2$ stimulation in
500 comparison to control treated cells, as determined by RNA-Seq analysis. DEG criteria:
501 FPKM ≥ 1 after treatment; fold change ≥ 1.5 or ≤ 0.67 (n = 3 biologically independent
502 experiments). (C) Examples of genes identified as differentially expressed by RNA-Seq
503 (n = 3 biologically independent experiments; mean values ± SEM). (D) Number of genes
504 containing at least one pCREB peak in the proximity after dmPGE$_2$ stimulation. pCREB
505 peaks were assigned to a gene when located within a window from -5kb upstream of the
506 transcription start site (TSS) to +5kb downstream of the TTS was considered (n = 2
507 biologically independent ChIP-Seq experiments). (E) Correlation between pCREB
508 binding and gene expression in response to dmPGE$_2$. pCREB density was calculated by
509 dividing the total number of pCREB peaks associated to each gene category (up-, down,
510 and nonregulated genes) by the total amount of base pairs that this category occupies in
511 the genome. pCREB peaks were assigned to a gene when located from +5 kb upstream
512 of the TSS to +5kb downstream of the TTS. Peak density in the genome was calculated
513 by considering random distribution of pCREB sites in the whole genome. (F) Genomic
514 distribution of unique pCREB peaks (inducible; present only after dmPGE$_2$ stimulation)
515 versus ubiquitous pCREB peaks. (G) Enrichment of pCREB binding at 4 representative
516 dmPGE$_2$ response genes: CXCL2 (promoter, intergenic), CXCL8 (promoter, intergenic),
517 PDE4B (intronic), and FOSL2 (promoter, intronic). Gray bars indicate intronic and
518 intergenic pCREB peaks. Genomic location of presented window is indicated at the
519 bottom of the panels.
520

18

521 **Figure 2.**

19
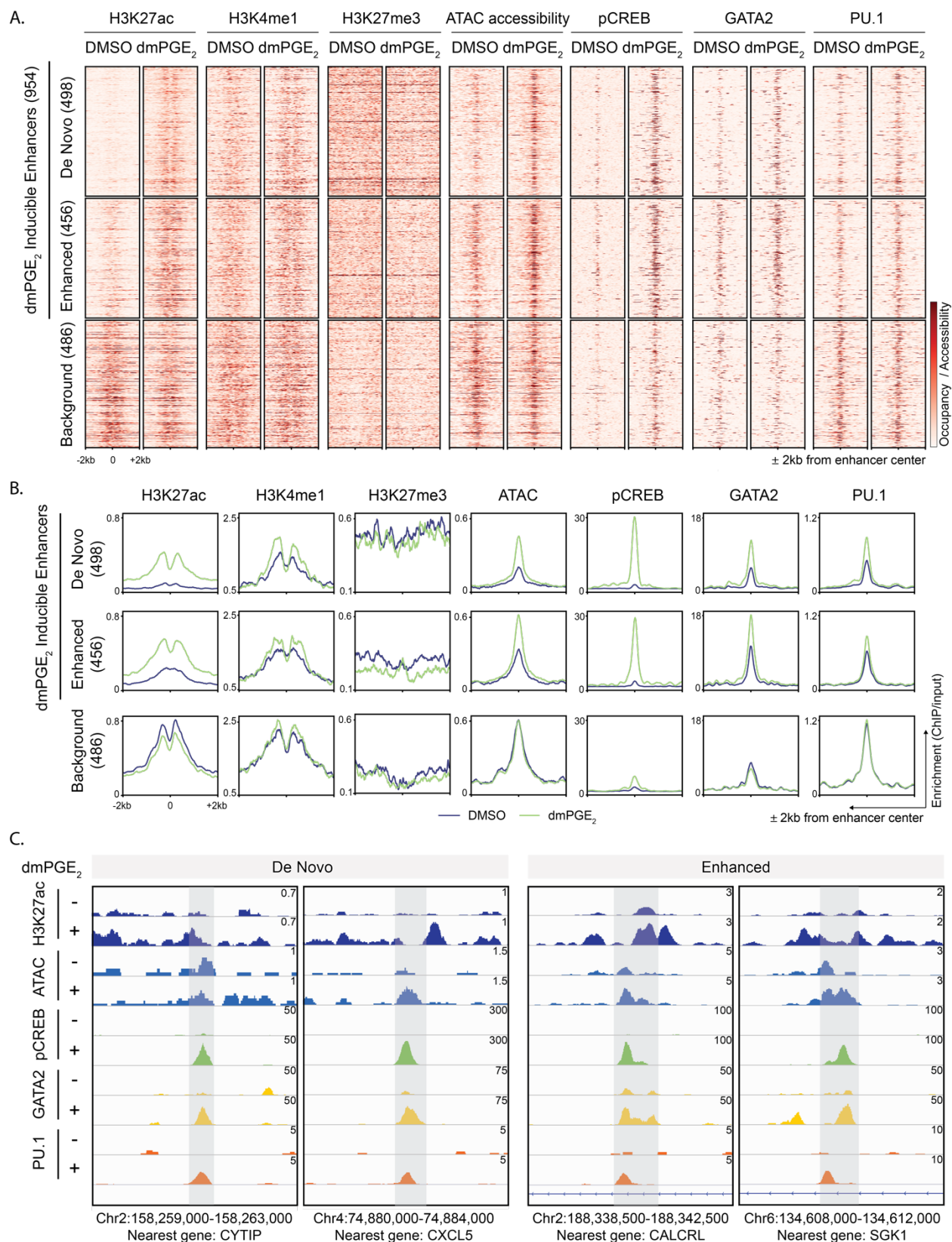
523 **Figure 2. Stimuli-responsive enhancers gain chromatin accessibility and**
524 **transcription factor binding after dmPGE$_2$ stimulation.** (A, B) Heat maps (A) and
525 average enrichment profiles (B) of histone marks, ATAC accessibility and transcription
526 factors at enhancers before and after dmPGE$_2$ treatment. H3K27ac enriched regions
527 identified by ChIP-Seq are classified as De Novo, Enhanced or Background enhancers
528 according to the change in H3K27ac levels observed following dmPGE$_2$ stimulation (n =
529 2 biologically independent experiments). A randomly sampled, comparable number of
530 background enhancers (486) is shown. (C) Enrichment of histone mark, ATAC
531 accessibility and transcription factor binding in response to dmPGE$_2$ at 4 representative
532 stimuli-response enhancers. Genomic location of presented window and nearest gene
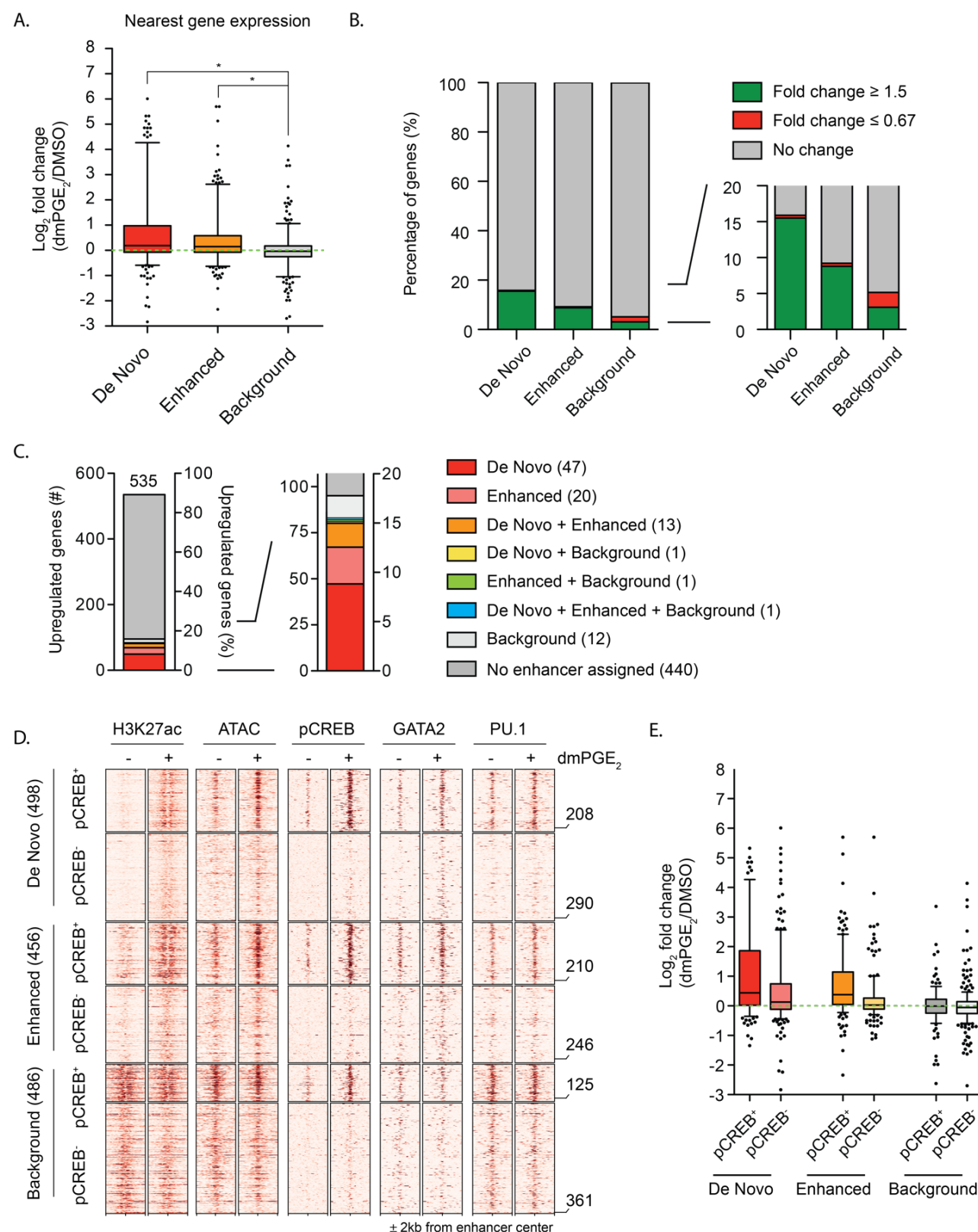533 are indicated at the bottom of the panel.
534

535 **Figure 3.**

536
537

538   **Figure 3. Stimuli-responsive enhancers mediate dmPGE$_2$-induced gene expression**

539   **changes.** (A) Gene expression changes of genes associated with stimuli-responsive and

540   background enhancers. Enhancers were assigned to an individual nearest gene. Only

541   genes with a mapped TSS within 15kb of an enhancer were considered. Box plots shows

542   median, 25th and 75th percentiles, whiskers are from 5th and 95th percentiles. Dots indicate

543   outliers. (B) Percentages of enhancer nearest genes with fold changes in expression $\geq$

544   1.5-fold or $\leq$ 0.67-fold for each enhancer category. (C) Upregulated genes with a fold

545   change in expression $\geq$ 1.5 (535) and their associated enhancers. (D) Heat maps of

546   H3K27ac, ATAC accessibility and transcription factors around enhancers before and after

547   dmPGE$_2$ treatment. De Novo, Enhanced or Background enhancers were subset based

548   on the presence or absence of pCREB after dmPGE$_2$. A randomly sampled, comparable

549   number of background enhancers (486) is shown. Numbers of enhancers within each

550   subset is indicated on the right of the heatmap. (E) Gene expression changes of genes

551   associated with pCREB positive and pCREB negative enhancers. Enhancers were

552   assigned to an individual nearest gene. Only genes with a mapped TSS within 15kb of an

553   enhancer were considered. Box plots shows median, 25th and 75th percentiles, whiskers

554   are from 10th and 90th percentiles. Dots indicate outliers. For all analysis presented here

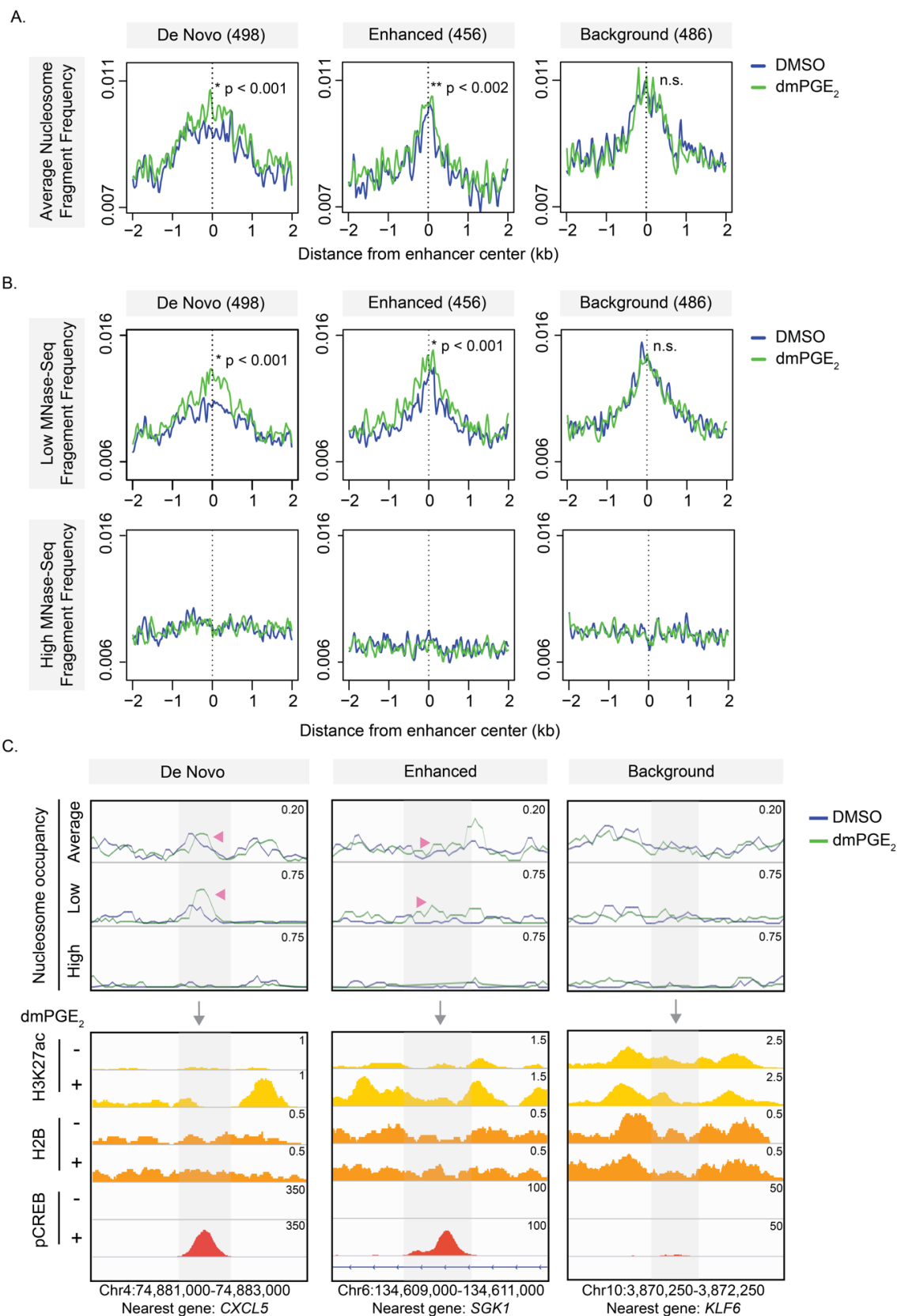555   a randomly sampled set of background enhancers (486) was used.

22

556 **Figure 4.**

557

558 **Figure 4. dmPGE$_2$-responsive enhancers retain accessible nucleosomes after**

559 **stimulation.** (A) Average nucleosome occupancy profiles at stimuli-responsive and

560 background enhancers from 4 MNase titration points. (n = 3 biologically independent

561 MNase-Seq experiments). (B) Nucleosome profiles of low- and high MNase-Seq at

562 stimuli-responsive and background enhancers (n = 3 biologically independent

563 experiments). P-values by Wilcoxon rank-sum test. (C) Nucleosome fragment frequency

564 and enrichment of H3K27ac, H2B, and pCREB at 3 representative stimuli-responsive and

565 background enhancers. Genomic location of presented window and nearest gene are

566 indicated at the bottom of the panel. Genomic location of presented window and enhancer

567 nearest gene are indicated at the bottom of the panel. For all analysis presented here a

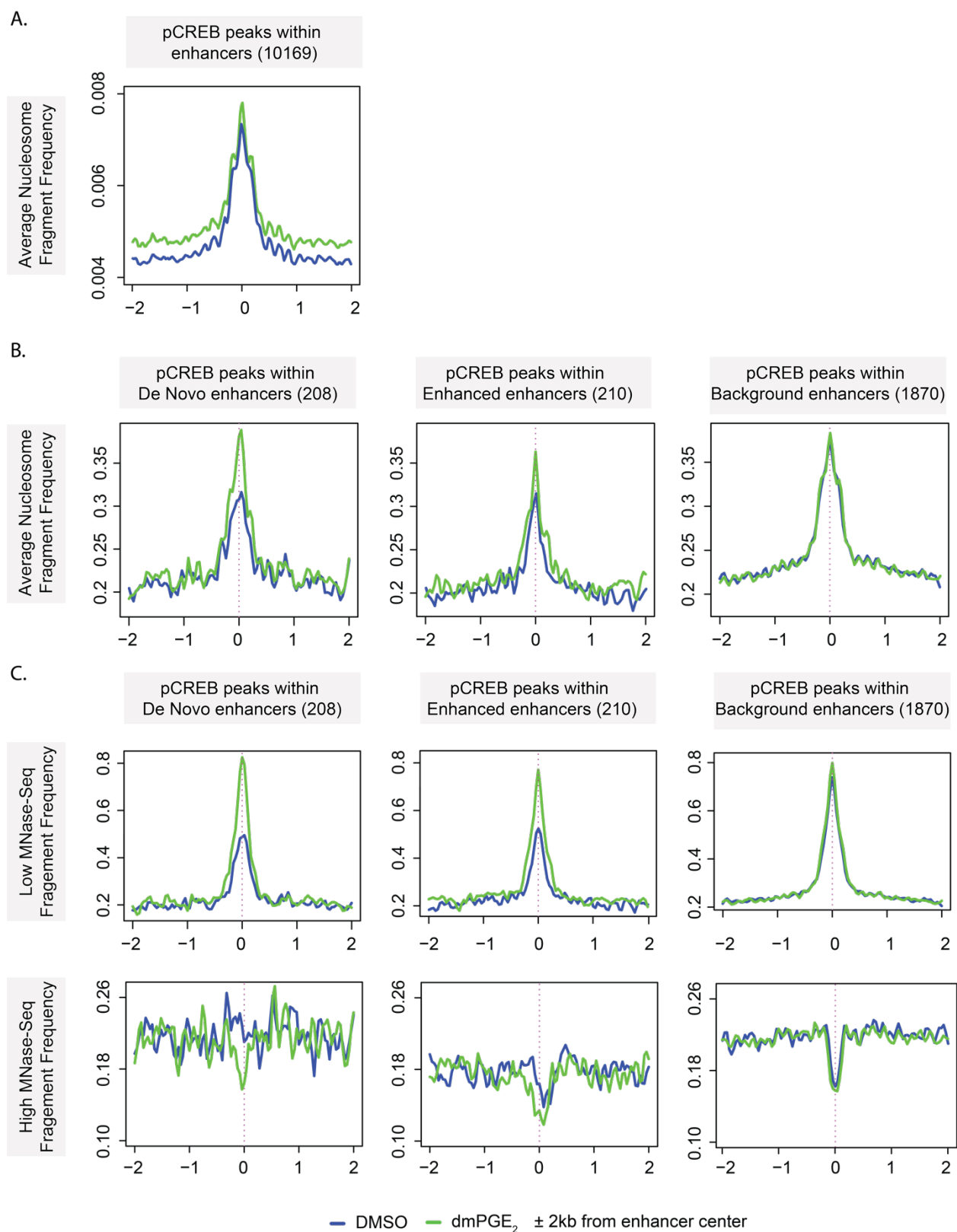568 randomly sampled set of background enhancers (486) was used.

569 **Figure 5.**

570
571

572 **Figure 5. pCREB engages accessible nucleosomes in stimuli-responsive**

573 **enhancers.** (A) Average nucleosome frequency at pCREB peaks located within

574 enhancers before and after dmPGE$_2$ stimulation (n = 3 biologically independent MNase-

575 Seq experiments). (B) Averaged nucleosome occupancy profiles at pCREB-bound sites

576 within stimuli-responsive and background enhancers from 4 MNase titration points (n = 3

577 biologically independent experiments). (C) Nucleosome profiles of low- and high MNase-

578 Seq at pCREB-bound sites within stimuli-responsive and background enhancers (n = 3

579 biologically independent experiments). For all analysis presented here a randomly

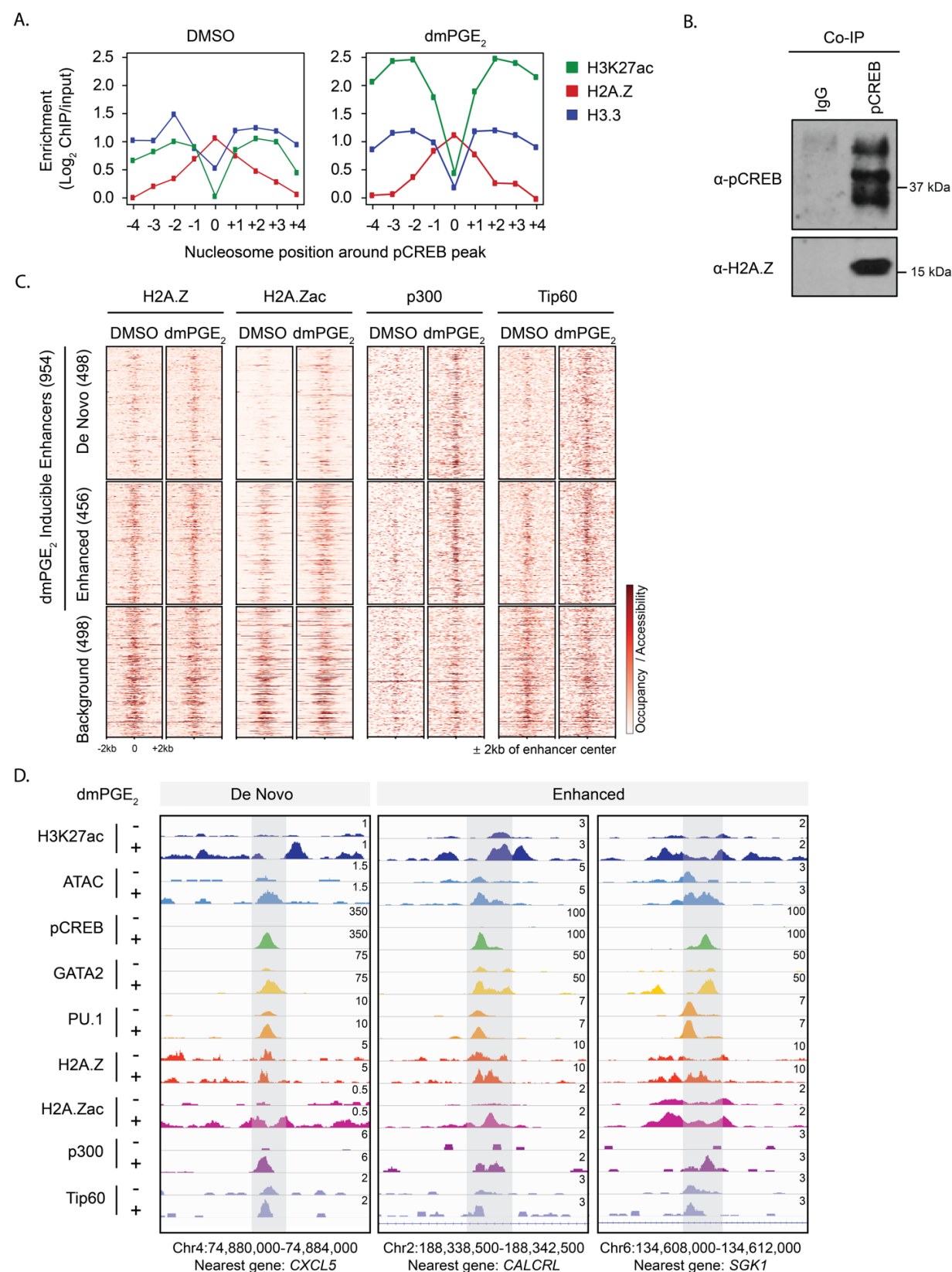580 sampled set of background enhancers (486) was used.

581 **Figure 6.**

582

27

583 **Figure 6. Modification of H2A.Z-variant accessible nucleosomes at stimuli-**

584 **responsive enhancers by HATs p300 and Tip60.** (A) Enrichment of histone variants at

585 nucleosome positions surrounding pCREB peaks within enhancers before and after

586 dmPGE$_2$ stimulation. Position 0 indicates the nucleosome overlapping with pCREB peak

587 centers. (B) Complex immunoprecipitation (Co-IP) showing that pCREB associated with

588 H2A.Z in U937 myeloid leukemia cells (n = 3 biologically independent experiments). (C)

589 Heat maps of H2A.Z, H2A.Zac, p300, and Tip60 binding at enhancers before and after

590 dmPGE$_2$ treatment. H3K27ac enriched regions identified by ChIP-Seq are classified as

591 De Novo, Enhanced or Background enhancers according to the change in H3K27ac

592 levels observed following dmPGE$_2$ stimulation (n = 2 biologically independent

593 experiments). (D) Enrichment of chromatin binding factors and transcription factors in

594 response to dmPGE$_2$ at 3 representative stimuli-response enhancers. Genomic location

595 of presented window and enhancer nearest gene are indicated at the bottom of the panel.

596 For all analysis presented here a randomly sampled set of background enhancers (486)

597 was used.

598

Materials and methods

Expansion of CD34+ cells

Human CD34+ hematopoietic stem and progenitor cells (HSPCs), isolated from peripheral blood of granulocyte colony-stimulating factor (G-CSF) mobilized healthy volunteers, were purchased from the Fred Hutchinson Cancer Research Center. The cells were maintained in suspension culture as previously described by Trompouki *et al.,* 2011[30]. Briefly, the cells were expanded in StemSpan medium (Stem Cell Technologies Inc.) supplemented with StemSpan CC100 cytokine mix (Stem Cell Technologies Inc.) and 2% Penicillin-Streptomycin for a total of 6 days.

Cell culture

U937 cells were maintained in suspension culture in RPMI-1640 supplemented with 10% (v/v) heat-inactivated fetal bovine serum, 1X Glutamax and 1% Penicillin-Streptomycin at 37° in a humidified atmosphere of 5% CO_2.

dmPGE$_2$ treatment

16,16-dimethyl prostaglandin E2 was purchased reconstituted in DMSO from Cayman Chemicals (cat. #14750), aliquoted and stored in -80°C until use. Cells were counted, collected and resuspended in StemSpan medium with 2% PenStrep (CD34+ Cells) or RPMI with 1% Penicillin-Streptomycin, but in the absence of additional cytokines or growth factors. Cells were treated with dmPGE$_2$ (Cayman chemicals) or DMSO (vehicle control) for 2 hours.

qPCR analysis

RNA was extracted from using the RNeasy plus mini kit (Qiagen). cDNA synthesis was performed using the Superscript VILO (Invitrogen) and using equal amounts of starting RNA. The cDNA was analyzed with the Light Cycler 480 II SYBR green master mix (Applied Biosystems), and the QuantStudio 12K Flex (Applied Biosystems). All samples were prepared in triplicate. The PCR cycle conditions used are: (a) 95°C for 5 min, (b)

29

629   [95°C for 10 sec, 54°C for 10 sec, 72°C for 15 sec] X 40 cycles. The analysis of Ct values

630   were performed using $2^{\wedge}-\Delta\Delta T$ method. The PCR primer-pairs used are:

631

632   CXCL2   Fwd: AAACCGAAGTCATAGCCACACTC

633   Rev: AGCCACCAATAAGCTTCCTCCTTC

634   CXC4   Fwd: CCTATGCAAGGCAGTCCATGT

635   Rev: GGTAGCGGTCCAGACTGATGA

636   EGR1   Fwd: GCGAGCAGCCCTACGAGCAC

637   Rev: TGCAGGCTCCAGGGAAAAGC

638   FOS   Fwd: TGCCTCTCCTCAATGACCCTGA

639   Rev: ATAGGTCCATGTCTGGCACGGA

640   FOSB   Fwd: TTCTGACTGTCCCTGCCAAT

641   Rev: CGGGGTCAGATGCAAAATAC

642   FOSL2   Fwd: GCAGTTGGGTTTCTGGCTTGAG

643   Rev: TCCTGCTACTCCTGGCTCATTC

644   GAPDH   Fwd: GAAGGTCGGAGTCAACGGATTT

645   Rev: GAATTTGCCATGGGTGGAAT

646   ICER   Fwd: CACCATGGCTGTAACTGGAGATGAC

647   Rev: AGGTCCAAGTCAAAGACAGTTACTC

648   NR4A1   Fwd: GAGTGCACAGAAGAACT

649   Rev: CACAGGAGGAGGAAGA

650   NR4A2   Fwd: CACAGGTTGCAATGCGTTCG

651   Rev: TCAATTATTGCTGGCGGTGG

652   NR4A3   Fwd: CGTCGAAACCGATGTCAGTA

653   Rev: GACGACCTCTCCTCCCTTTC

654   PTGS2   Fwd: GAATCATTCACCAGGCAAATTG

655   Rev: TCTGTACTGCGGGTGGAACA

656

657   *Western blotting*

658   Cells were treated for 2 hours, washed in 1X PBS, and collected in RIPA buffer with

659   protease and phosphatase inhibitors. Samples were run on acrylamide gel and

660　transferred onto a nitrocellulose membrane. Membrane was blocked for one hour in 5%

661　of milk or TBS-T and incubated overnight at 4ºC with anti-vinculin (Abcam 73412), anti-

662　CREB (Santa Cruz SC-186), anti-pCREB (Ser133, Cell Signalling #9198), anti-H2A.Z

663　(Abcam 4174), or anti-IgG (Cell Signalling #2729). The next day, membranes were

664　washed, incubated with HRP-conjugated secondary antibodies for 1 hour at room

665　temperature, and developed with SuperSignal West Pico Plus Chemiluminescent

666　substrate.

667

668　*Co-immunoprecipitation (Co-IP)*

669　Co-IP was performed as previously described by Santoriello *et al.,* 2020[76]. Cells were

670　washed twice with 1X PBS. Nuclei were isolated with 0.05% Triton in PBS and lysed in

671　nuclei lysis buffer (20mM Hepes-KOH pH7.9, 25% glycerol, 420mM NaCl, 1.5mM MgCl2,

672　0.2mM EDTA, 0.5mM DTT). 500ug of protein extracts was used and the salt

673　concentration was diluted from 420mM to 150mM NaCl using 20mM Hepes-KOH pH7.9,

674　20% glycerol, 0.25mM EDTA, 0.05% NP-40. Cell lysates were pre-cleared with non-

675　antibody bounds beads for 1 hour at 4°C. Antibody bounds protein G Dynabeads were

676　added to pre-cleared lysate and samples incubated overnight at 4°C. Antibodies used:

677　IgG (Cell Signalling #2729), phospho-CREB (Ser133, Cell Signalling #9198). Protein-

678　bead complexes were then washed 5 times with wash buffer (20mM Hepes-KOH pH7.9,

679　10% Glycerol, 150mM NaCl, 1.5 MgCl2, 0.2mM EDTA, 0.5mM DTT) and beads were

680　boiled in 50μL Laemmli Buffer for 15min at 95°C to elute proteins. Subsequently, samples

681　were subjected to western blot.

682

683　*RNA-Seq*

684　RNA from one million cells was isolated using the RNeasy plus mini kit (Qiagen #74134).

685　5μg of RNA was subjected to ribosomal and mitochondrial RNA depletion using the

686　RiboZero Gold kit (Human/Mouse/Rat, Epicentre #MRZG12324) according to

687　manufacturer's instructions. The ribo-zero treated RNA wa*s* used to create multiplexed

688　RNA-Seq libraries using the NEBNext Ultra RNA Library Prep Kit (Illumina E7530)

689　according to the manufacturer's instructions. Briefly 500pg of ribozero treated RNA was

690　fragmented and used to produce cDNA libraries using the NEBnext Ultra RNA library prep

691   kit (NEB, E7530S) according to the manufacturer's protocol. Purified double-stranded

692   cDNA underwent end-repair and dA-tailing reactions following manufacturer's reagents

693   and reaction conditions. The obtained DNAs were used for Adaptor Ligation using

694   adaptors and enzymes provided in NEBNext Multiplex Oligos for Illumina (NEB #E7335)

695   and following recommended reaction conditions. Eluted DNA was enriched with PCR

696   reaction using Fusion High-Fidelity PCR Master Mix kit (NEB, M0531S) and specific index

697   primers supplied in NEBNext Multiplex Oligo Kit for Illumina (Index Primer Set 1, NEB,

698   E7335L). Conditions for PCR used are as follows: 98°C, 30 sec; [98°C, 10 sec; 65°C, 30

699   sec; 72°C, 30 sec] X 15 cycles; 72°C, 5 min; hold at 4°C. PCR reaction mix was purified

700   using Agencourt AMPure XP beads (1X of reaction volume). Libraries were eluted in 20µl

701   elution buffer. All the libraries went through quality control analysis using an Agilent

702   Bioanalyzer and subjected to next-generation sequencing using Illumina Hiseq 2500

703   platform. Quality control of RNA-Seq datasets was performed by FastQC and Cutadapt

704   to remove adaptor sequences and low-quality regions. The high-quality reads were

705   aligned to UCSC hg19 for human using Tophat 2.0.11 without novel splicing form calls.

706   Transcript abundance and differential expression were calculated with Cufflinks 2.2.1.

707   FPKM values were used to normalize and quantify each transcript.

708

709   *ChIP-Seq*

710   For ChIP-Seq experiments the following antibodies were used: H3K27ac (Abcam

711   ab4729), H3K4me1 (Abcam ab8895), H3K27me3, (Abcam ab195477), pCREB (Ser133,

712   Cell Signalling #9198), GATA2 (Santa Cruz sc9008X), H2A.Z (Abcam ab4174), H2A.Zac

713   (Abcam ab18262), H2B (Abcam ab1790), H3.3 (Milipore #09-838), H4 (Abcam ab7311),

714   p300 (Millipore #05-257), and Tip60 (generous gift from Bruno Amati). ChIP experiments

715   were performed as previously described by Trompouki *et al.,* 2011[30]. Briefly, 20 million

716   cells were crosslinked by the addition of 1/10 volume 11% fresh formaldehyde for 10 min

717   at room temperature. The crosslinking was quenched by the addition of 1/20 volume 2.5M

718   glycine for 5 minutes. Cells were washed twice with ice-cold PBS. Cells were lysed in

719   10mL of Lysis buffer 1 (50mM HEPES-KOH, pH 7.5, 140mM NaCl, 1mM EDTA, 10%

720   glycerol, 0.5% NP-40, 0.25% Triton X-100, plus protease and phosphatase inhibitors) for

721   10 min at 4°C. After centrifugation, cells were resuspended in 10 mL of Lysis buffer 2

722 (10mM Tris-HCl, pH 8.0, 200mM NaCl, 1mM EDTA, 0.5mM EGTA, plus protease and
723 phosphatase inhibitors) for 10 min at room temperature. Cells were pelleted and
724 resuspended in 3mL of sonication buffer (10mM Tris-HCl, pH 8.0, 100mM NaCl, 1mM
725 EDTA, 0.5mM EGTA, 0.1% Na-Deoxycholate, 0.05% N-lauroylsarcosine, plus protease
726 and phosphatase Inhibitors) and sonicated in a Bioruptor sonicator for 36 cycles of 30 sec
727 each followed by a 1min resting interval. Samples were centrifuged for 10min at 18,000g
728 and 1% Triton-X was added to the supernatant. Prior to the immunoprecipitation, 50mL
729 of protein G beads (Invitrogen 100-04D) for each reaction were washed twice with PBS,
730 0.5% BSA twice. Finally, the beads were resuspended in 250µL of PBS, 0.5% BSA and
731 5µg of each antibody. Beads were rotated for at least 6 hours at 4°C and then washed
732 twice with PBS with 0.5% BSA. Cell lysates were added to the beads and incubated at
733 4°C overnight. Beads were washed 1x with (20mM Tris-HCl. pH 8, 150mM NaCl, 2mM
734 EDTA, 0.1% SDS, 1% Triton X-100), 1x with (20mM Tris-HCl, pH 8, 500mM NaCl, 2mM
735 EDTA, 0.1% SDS, 1% Triton X-100), 1x with (10mM Tris-HCl, pH 8, 250nM LiCl, 2mM
736 EDTA, 1% NP4-0) and 1x with TE and finally resuspended in 200µL elution buffer (50mM
737 Tris-Hcl, pH 8.0, 10mM EDTA, 0.5%–1% SDS). 50µL of cell lysates prior to addition to
738 the beads was kept as input. Crosslinking was reversed by incubating samples at 65°C
739 for at least 6 hours. Afterwards the cells were treated with RNase and proteinase K and
740 the DNA was extracted by Phenol/Chloroform extraction.

741 ChIP-Seq libraries were prepared using the following protocol. End repair of
742 immunoprecipitated DNA was performed using the End-It End-Repair kit (Epicentre,
743 ER81050) and incubating the samples at 25°C for 45 min. End-repaired DNA was purified
744 using AMPure XP Beads (1.8X of the reaction volume) (Agencourt AMPure XP – PCR
745 purification Beads, BeckmanCoulter, A63881) and separating beads using DynaMag-96
746 Side Skirted Magnet (Life Technologies, 12027). A-tails were added to the end-repaired
747 DNA using NEB Klenow Fragment Enzyme (3'-5' exo, M0212L), 1X NEB buffer 2 and
748 0.2mM dATP (Invitrogen, 18252-015) and by incubating the reaction mix at 37µC for 30
749 min. A-tailed DNA was cleaned up using AMPure beads (1.8X of reaction volume).
750 Subsequently, cleaned up A-tailed DNA went through Adaptor ligation reaction using
751 Quick Ligation Kit (NEB, M2200L) following manufacturer's protocol. Adaptor-ligated DNA
752 was first cleaned up using AMPure beads (1.8X of reaction volume), eluted in 100µl and

753 then size-selected using AMPure beads (0.9X of the final supernatant volume, 90µl).

754 Adaptor-ligated DNA fragments of proper size were enriched with PCR reaction using

755 Fusion High-Fidelity PCR Master Mix kit (NEB, M0531S) and specific index primers

756 supplied in NEBNext Multiplex Oligo Kit for Illumina (Index Primer Set 1, NEB, E7335L).

757 Conditions for PCR used are as follows: 98°C, 30 sec; [98°C, 10 sec; 65°C, 30 sec; 72°C,

758 30 sec] X 15 to 18 cycles; 72°C, 5 min; hold at 4°C. PCR enriched fragments were cleaned

759 up using AMPure beads (1X of reaction volume). Libraries were eluted in 20µl elution

760 buffer. All the libraries went through quality control analysis using an Agilent Bioanalyzer

761 and subjected to next-generation sequencing using Illumina Hiseq 2500 platform. All the

762 libraries went through quality control analysis using an Agilent Bioanalyzer and subjected

763 to next-generation sequencing using Illumina Hiseq 2500 platform. All ChIP-Seq datasets

764 were aligned to UCSC build version hg19 of the human genome using Bowtie2 (version

765 2.2.1; Langmead *et al.,* 2012[77]) with the following parameters: -end-to-end, -N0, -L20. We

766 used the MACS2 version 2.1.0 (Zhang *et al.,* 2008[78]) peak-finding algorithm to identify

767 regions of ChIP-Seq peaks, with a q-value threshold of enrichment of 0.05 and false

768 discovery rate of < 0.01 for all datasets. The genome-wide occupancy profile figures were

769 generated by deeptools (Ramirez *et al.,* 2016[79]) using the reference-point mode and the

770 scale-regions mode. The genomic distribution of peaks was plotted using the ChIPSeeker

771 R package, annotatePeak to assign peaks to a genomic annotation, which includes

772 whether a peak is in the TSS, Exon, 5' UTR, 3' UTR, Intronic or Intergenic. The

773 genome annotation is from the R-bioconductor annotation packages. Heat maps of the

774 ChIP-Seq binding were generated using the input normalized results of the MACS peak

775 calling output. The outputted bedGraph files were converted to BigWig files. Those files-

776 were then processed using computeMatrix and plotHeatmap tools within the deeptools

777 3.0 package. Enhancers were assigned to genes using GREAT to the nearest genes

778 within 15kb of peaks.

779

780 *Defining Enhancer Categories*

781 We used the SPP package to call clusters of H3K27ac enrichment, normalized to input,

782 from ChIP-Seq data (Kharchenko *et al.,* 2008[80]). Regions within 500bp of each other were

783 merged and only regions reproduced between two independent biological H3K27ac ChIP-

34

784   Seq replicates (in either sample dmPGE$_2$ or DMSO) were included for further analysis.

785   Enhancers were defined as TSS distal H3K27ac regions that are $\geq$ 1kb in length and

786   located $\geq$ 2kb away from TSS. This yielded a total of 25,998 H3K27ac enriched ChIP-

787   Seq regions, here named enhancers. P-value was computed using paired t-test between

788   dmPGE$_2$ and DMSO on enrichment values for every region.

789   Called enhancers were classified based on the three following criteria and using cut-off

790   described in the table below: (1) H3K27ac enrichment in each replicate in each condition,

791   (2) delta H3K27ac enrichment upon stimulation, (3) p-value of Δ H3K27ac enrichment. All

792   regions not classified as not meeting above mentioned criteria were classified as

793   'Background' enhancers.

794

	H3K27ac Enrichment		Δ Enrichment	Significance
	DMSO	dmPGE$_2$	[dmPGE$_2$-DMSO]	p-value
De Novo	≤ 1	≥ 2	≥ 1	≤ 0.05
Enhanced	≥ 1	≥ 3	≥ 2	≤ 0.05

795

796   *ATAC-Seq*

797   50.000 cells per condition were harvested by spinning at 500g for 5 min, 4°C. Cells were

798   washed once with 50µl of cold 1X PBS and spun down at 500g for 5 min, 4°C. After

799   discarding supernatant, cells were lysed using 50µl cold lysis buffer (10mM Tris-HCl pH

800   7.4, 10mM NaCl, 3 mM MgCl$_2$, 0.1% IGEPAL) and spun down immediately at 500g for 10

801   min at 4°C. Then the cells were precipitated and kept on ice and subsequently

802   resuspended in 25µl 2X Tagment DNA Buffer (Illumina Nextera kit), 2.5µl Transposase

803   enzyme (Illumina Nextera kit, 15028252) and 22.5µl Nuclease-free water in a total of 50uL

804   reaction for 1 hour at 37°C. DNA was then purified using Qiagen MinElute PCR

805   purification kit (28004) in a final volume of 10µl. Libraries were constructed according to

806   Illumina protocol using the DNA treated with transposase, NEB PCR master mix, Sybr

807   green, universal and library-specific Nextera index primers. The first round of PCR was

808   performed under the following conditions: 72°C, 5 min; 98°C, 30 sec; [98°C, 10 sec; 63°C,

809   30 sec; 72°C, 1 min] X 5 cycles; hold at 4°C. Reactions were kept on ice and using a 5µL

810   reaction aliquot, the appropriate number of additional cycles required for further

811   amplification was determined in a side qPCR reaction: 98°C , 30 sec; [98°C, 10 sec; 63°C,

812   30 sec; 72°C, 1 min] X 20 cycles; hold at 4°C. Upon determining the additional number of

813   PCR cycles required further for each sample, library amplification was conducted using

814   the following conditions: 98°C, 30 sec; [98°C, 10 sec; 63°C, 30 sec; 72°C, 1 min] X

815   appropriate number of cycles; hold at 4°C. Libraries prepared went through quality control

816   analysis using an Agilent Bioanalyzer and then subjected to next generation sequencing

817   using Illumina Hiseq 2500 platform. We used the MACS2 version 2.1.0 (Zhang *et al.,*

818   2008[78]) peak-finding algorithm to identify regions of ATAC-Seq peaks, with the following

819   parameter -- nomodel --shift -100 --extsize 200. A q-value threshold of enrichment of 0.05

820   was used for all datasets.

821

822   *MNase-Seq*

823   CD34^{+} HSPC cells were crosslinked by the addition of 1/10 volume 11% fresh

824   formaldehyde for 10 min at room temperature. The crosslinking was quenched by the

825   addition of 1/20 volume 2.5M glycine for 5 minutes. Cells were washed twice with ice-cold

826   PBS. For MNase digestion, the nuclei pellet was resuspended in MNase digestion buffer

827   (50mM Tris, pH 7.4, 25mM KCl, 4mM MgCl2, 1mM CaCl2, 12.5% Glycerol and

828   COMPLETE protease inhibitors (Roche)). Digestion took place with 10^6 cells per titration

829   point in a volume of 500μl MNase digestion buffer. Either 1, 2, 4, 8, 16, 32, 64, 128 or 256

830   units of MNase (Worthington Biochemical) were added to pre-warmed nuclei and

831   incubated at 25 °C for 15 min. Digestion was halted with 25mM EDTA/EGTA and 0.5%

832   SDS and 125mM NaCl was added to the samples. Digestions were incubated with RNase

833   (Roche) for 1 hour at 37 °C, with proteinase K (Roche) for 1 hour at 55 °C, and cross-link

834   reversal was performed at 65 °C for 16 hours. DNA was purified by Phenol/Chloroform

835   extraction and ethanol precipitation. MNase digestion was evaluated on a 2% agarose

836   gel and fragments from four MNase concentrations representing 10%, 25%, 50% and

837   75% mono-nucleosomal fragments were individually prepared for next generation

838   sequencing. Ampure SPRI beads (Beckman Coulter) were used in a double size selection

839   with ratios of 0.7X and 1.7X to obtain a range of fragment sizes from ~100 to

840   1,000bp. DNA was eluted from the beads and used as input into the library preparation

841   protocol. DNA libraries were prepared for each individual titration point using the NEBNext

842   Ultra II DNA Library Prep Kit for Illumina (E7370, New England Biolabs) and barcoded

843   using NEBNext Multiplex Oligos for Illumina (Index Primers Set 1 & 2; New England

844   Biolabs). Number of PCR cycles was calculated using a real-time qPCR-based approach

845   (Lion *et al.,* 2020[81]). Libraries prepared went through quality control analysis using an

846   Agilent Bioanalyzer. Four barcoded titration libraries were pooled in one sample, and

847   paired-end sequencing on an Illumina Hiseq 2500 instrument was performed. Three

848   biological replicated were sequenced. The sequenced paired-end reads were mapped to

849   hg19 using Bowtie aligner v. 0.12.9. Only uniquely mapped reads with no more than two

850   mismatches were retained. The reads with the insert sizes <50 bp or >500 bp were filtered

851   out. Genomic positions with the numbers of mapped tags above the significance threshold

852   of Z-score=7 were identified as anomalous, and the tags mapped to such positions were

853   discarded. Read frequencies were computed in 300bp non-overlapping bins for each

854   titration point independently. The read frequencies were normalized by the corresponding

855   library sizes to represent values per one million of mapped reads. Nucleosome occupancy

856   analysis was carried out as previously described by Mieczkowski *et al.,* 2016[32].

857

Acknowledgments

Author Contributions

A.S., E.M.F, and M.E.M., performed experiments. M.P., B.M. and S.Y. performed bioinformatics analysis of next generation sequencing data. A.C., R.E.K., M.Y.T, and H. C. provided insights on data analysis and interpretation. A.S. and L.I.Z. managed the study and wrote the manuscript.

Conflict of Interests

L.I.Z. is founder and stockholder of Fate, Inc., Scholar Rock, Camp4 Therapeutics, Amagma Therapeutics and a scientific advisor for Stemgent. The other authors declare no competing interests.

References

1 North, T. E. *et al.* Prostaglandin E2 regulates vertebrate haematopoietic stem cell homeostasis. *Nature* **447**, 1007-1011, doi:10.1038/nature05883 (2007).

2 Cutler, C. *et al.* Prostaglandin-modulated umbilical cord blood hematopoietic stem cell transplantation. *Blood* **122**, 3074-3081, doi:10.1182/blood-2013-05-503177 (2013).

3 Morrison, S. J. & Scadden, D. T. The bone marrow niche for haematopoietic stem cells. *Nature* **505**, 327-334, doi:10.1038/nature12984 (2014).

4 Fast, E. M. *et al.* Niche signals regulate continuous transcriptional states in hematopoietic stem cells. *bioRxiv*, 2021.2003.2009.430613, doi:10.1101/2021.03.09.430613 (2021).

892 5   Vihervaara, A., Duarte, F. M. & Lis, J. T. Molecular mechanisms driving
893   transcriptional stress responses. *Nat Rev Genet* **19**, 385-397, doi:10.1038/s41576-
894   018-0001-6 (2018).
895 6   de Nadal, E., Ammerer, G. & Posas, F. Controlling gene expression in response
896   to stress. *Nat Rev Genet* **12**, 833-845, doi:10.1038/nrg3055 (2011).
897 7   Spitz, F. & Furlong, E. E. Transcription factors: from enhancer binding to
898   developmental control. *Nat Rev Genet* **13**, 613-626, doi:10.1038/nrg3207 (2012).
899 8   Natoli, G. Maintaining cell identity through global control of genomic organization.
900   *Immunity* **33**, 12-24, doi:10.1016/j.immuni.2010.07.006 (2010).
901 9   Kim, H. D. & O'Shea, E. K. A quantitative model of transcription factor-activated
902   gene expression. *Nat Struct Mol Biol* **15**, 1192-1198, doi:10.1038/nsmb.1500
903   (2008).
904 10   Klemm, S. L., Shipony, Z. & Greenleaf, W. J. Chromatin accessibility and the
905   regulatory epigenome. *Nat Rev Genet* **20**, 207-220, doi:10.1038/s41576-018-
906   0089-8 (2019).
907 11   Bell, O., Tiwari, V. K., Thoma, N. H. & Schubeler, D. Determinants and dynamics
908   of genome accessibility. *Nat Rev Genet* **12**, 554-564, doi:10.1038/nrg3017 (2011).
909 12   Miller, S. B. Prostaglandins in health and disease: an overview. *Semin Arthritis*
910   *Rheum* **36**, 37-49, doi:10.1016/j.semarthrit.2006.03.005 (2006).
911 13   Goessling, W. *et al.* Genetic interaction of PGE2 and Wnt signaling regulates
912   developmental specification of stem cells and regeneration. *Cell* **136**, 1136-1147,
913   doi:10.1016/j.cell.2009.01.015 (2009).
914 14   Hoggatt, J., Singh, P., Sampath, J. & Pelus, L. M. Prostaglandin E2 enhances
915   hematopoietic stem cell homing, survival, and proliferation. *Blood* **113**, 5444-5455,
916   doi:10.1182/blood-2009-01-201335 (2009).
917 15   Goessling, W. *et al.* Prostaglandin E2 enhances human cord blood stem cell
918   xenotransplants and shows long-term safety in preclinical nonhuman primate
919   transplant models. *Cell Stem Cell* **8**, 445-458, doi:10.1016/j.stem.2011.02.003
920   (2011).
921 16   Perlin, J. R., Sporrij, A. & Zon, L. I. Blood on the tracks: hematopoietic stem cell-
922   endothelial cell interactions in homing and engraftment. *J Mol Med (Berl)* **95**, 809-
923   819, doi:10.1007/s00109-017-1559-8 (2017).
924 17   Klein, T., Shephard, P., Kleinert, H. & Komhoff, M. Regulation of cyclooxygenase-
925   2 expression by cyclic AMP. *Biochim Biophys Acta* **1773**, 1605-1618,
926   doi:10.1016/j.bbamcr.2007.09.001 (2007).
927 18   Sinclair, A. *et al.* CXCR2 and CXCL4 regulate survival and self-renewal of
928   hematopoietic stem/progenitor cells. *Blood* **128**, 371-383, doi:10.1182/blood-2015-
929   08-661785 (2016).
930 19   Freire, P. R. & Conneely, O. M. NR4A1 and NR4A3 restrict HSC proliferation via
931   reciprocal regulation of C/EBPalpha and inflammatory signaling. *Blood* **131**, 1081-
932   1093, doi:10.1182/blood-2017-07-795757 (2018).
933 20   Santaguida, M. *et al.* JunB protects against myeloid malignancies by limiting
934   hematopoietic stem cell proliferation and differentiation without affecting self-
935   renewal. *Cancer Cell* **15**, 341-352, doi:10.1016/j.ccr.2009.02.016 (2009).

936 21 Antonchuk, J., Sauvageau, G. & Humphries, R. K. HOXB4-induced expansion of
937   adult hematopoietic stem cells ex vivo. *Cell* **109**, 39-45, doi:10.1016/s0092-
938   8674(02)00697-9 (2002).
939 22 Luan, B. *et al.* CREB pathway links PGE2 signaling with macrophage polarization.
940   *Proc Natl Acad Sci U S A* **112**, 15642-15647, doi:10.1073/pnas.1519644112
941   (2015).
942 23 Parker, D. *et al.* Phosphorylation of CREB at Ser-133 induces complex formation
943   with CREB-binding protein via a direct mechanism. *Mol Cell Biol* **16**, 694-703,
944   doi:10.1128/MCB.16.2.694 (1996).
945 24 Gonzalez, G. A. & Montminy, M. R. Cyclic AMP stimulates somatostatin gene
946   transcription by phosphorylation of CREB at serine 133. *Cell* **59**, 675-680,
947   doi:10.1016/0092-8674(89)90013-5 (1989).
948 25 Creyghton, M. P. *et al.* Histone H3K27ac separates active from poised enhancers
949   and predicts developmental state. *Proc Natl Acad Sci U S A* **107**, 21931-21936,
950   doi:10.1073/pnas.1016071107 (2010).
951 26 Malik, A. N. *et al.* Genome-wide identification and characterization of functional
952   neuronal activity-dependent enhancers. *Nat Neurosci* **17**, 1330-1339,
953   doi:10.1038/nn.3808 (2014).
954 27 Ostuni, R. *et al.* Latent enhancers activated by stimulation in differentiated cells.
955   *Cell* **152**, 157-171, doi:10.1016/j.cell.2012.12.018 (2013).
956 28 Zhang, B. *et al.* A dynamic H3K27ac signature identifies VEGFA-stimulated
957   endothelial enhancers and requires EP300 activity. *Genome Res* **23**, 917-927,
958   doi:10.1101/gr.149674.112 (2013).
959 29 Thurman, R. E. *et al.* The accessible chromatin landscape of the human genome.
960   *Nature* **489**, 75-82, doi:10.1038/nature11232 (2012).
961 30 Trompouki, E. *et al.* Lineage regulators direct BMP and Wnt pathways to cell-
962   specific programs during differentiation and regeneration. *Cell* **147**, 577-589,
963   doi:10.1016/j.cell.2011.09.044 (2011).
964 31 John, S. *et al.* Chromatin accessibility pre-determines glucocorticoid receptor
965   binding patterns. *Nat Genet* **43**, 264-268, doi:10.1038/ng.759 (2011).
966 32 Mieczkowski, J. *et al.* MNase titration reveals differences between nucleosome
967   occupancy and chromatin accessibility. *Nat Commun* **7**, 11485,
968   doi:10.1038/ncomms11485 (2016).
969 33 Iwafuchi-Doi, M. *et al.* The Pioneer Transcription Factor FoxA Maintains an
970   Accessible Nucleosome Configuration at Enhancers for Tissue-Specific Gene
971   Activation. *Mol Cell* **62**, 79-91, doi:10.1016/j.molcel.2016.03.001 (2016).
972 34 Mueller, B. *et al.* Widespread changes in nucleosome accessibility without
973   changes in nucleosome occupancy during a rapid transcriptional induction. *Genes
974   Dev* **31**, 451-462, doi:10.1101/gad.293118.116 (2017).
975 35 Petesch, S. J. & Lis, J. T. Overcoming the nucleosome barrier during transcript
976   elongation. *Trends Genet* **28**, 285-294, doi:10.1016/j.tig.2012.02.005 (2012).
977 36 Zhang, Y. *et al.* Canonical nucleosome organization at promoters forms during
978   genome activation. *Genome Res* **24**, 260-266, doi:10.1101/gr.157750.113 (2014).
979 37 Schones, D. E. *et al.* Dynamic regulation of nucleosome positioning in the human
980   genome. *Cell* **132**, 887-898, doi:10.1016/j.cell.2008.02.022 (2008).

981 38 Valouev, A. *et al.* Determinants of nucleosome organization in primary human
982   cells. *Nature* **474**, 516-520, doi:10.1038/nature10002 (2011).
983 39 Ramani, V., Qiu, R. & Shendure, J. High Sensitivity Profiling of Chromatin
984   Structure by MNase-SSP. *Cell Rep* **26**, 2465-2476 e2464,
985   doi:10.1016/j.celrep.2019.02.007 (2019).
986 40 Ballare, C. *et al.* Nucleosome-driven transcription factor binding and gene
987   regulation. *Mol Cell* **49**, 67-79, doi:10.1016/j.molcel.2012.10.019 (2013).
988 41 Talbert, P. B. & Henikoff, S. Histone variants--ancient wrap artists of the
989   epigenome. *Nat Rev Mol Cell Biol* **11**, 264-275, doi:10.1038/nrm2861 (2010).
990 42 Brunelle, M. *et al.* The histone variant H2A.Z is an important regulator of enhancer
991   activity. *Nucleic Acids Res* **43**, 9742-9756, doi:10.1093/nar/gkv825 (2015).
992 43 Chen, P. *et al.* H3.3 actively marks enhancers and primes gene transcription via
993   opening higher-ordered chromatin. *Genes Dev* **27**, 2109-2124,
994   doi:10.1101/gad.222174.113 (2013).
995 44 Hu, G. *et al.* H2A.Z facilitates access of active and repressive complexes to
996   chromatin in embryonic stem cell self-renewal and differentiation. *Cell Stem Cell*
997   **12**, 180-192, doi:10.1016/j.stem.2012.11.003 (2013).
998 45 Jin, C. & Felsenfeld, G. Nucleosome stability mediated by histone variants H3.3
999   and H2A.Z. *Genes Dev* **21**, 1519-1529, doi:10.1101/gad.1547707 (2007).
1000 46 Giaimo, B. D., Ferrante, F., Herchenrother, A., Hake, S. B. & Borggrefe, T. The
1001   histone variant H2A.Z in gene regulation. *Epigenetics Chromatin* **12**, 37,
1002   doi:10.1186/s13072-019-0274-9 (2019).
1003 47 Adam, M., Robert, F., Larochelle, M. & Gaudreau, L. H2A.Z is required for global
1004   chromatin integrity and for recruitment of RNA polymerase II under specific
1005   conditions. *Mol Cell Biol* **21**, 6270-6279, doi:10.1128/MCB.21.18.6270-6279.2001
1006   (2001).
1007 48 Gevry, N. *et al.* Histone H2A.Z is essential for estrogen receptor signaling. *Genes*
1008   *Dev* **23**, 1522-1533, doi:10.1101/gad.1787109 (2009).
1009 49 Gavaravarapu, S. & Kamine, J. Tip60 inhibits activation of CREB protein by protein
1010   kinase A. *Biochem Biophys Res Commun* **269**, 758-766,
1011   doi:10.1006/bbrc.2000.2358 (2000).
1012 50 Vo, N. & Goodman, R. H. CREB-binding protein and p300 in transcriptional
1013   regulation. *J Biol Chem* **276**, 13505-13508, doi:10.1074/jbc.R000025200 (2001).
1014 51 Numata, A. *et al.* Lysine acetyltransferase Tip60 is required for hematopoietic stem
1015   cell maintenance. *Blood* **136**, 1735-1747, doi:10.1182/blood.2019001279 (2020).
1016 52 Sandberg, M. L. *et al.* c-Myb and p300 regulate hematopoietic stem cell
1017   proliferation and differentiation. *Dev Cell* **8**, 153-166,
1018   doi:10.1016/j.devcel.2004.12.015 (2005).
1019 53 Rebel, V. I. *et al.* Distinct roles for CREB-binding protein and p300 in hematopoietic
1020   stem cell self-renewal. *Proc Natl Acad Sci U S A* **99**, 14789-14794,
1021   doi:10.1073/pnas.232568499 (2002).
1022 54 Colino-Sanguino, Y. *et al.* A Read/Write Mechanism Connects p300 Bromodomain
1023   Function to H2A.Z Acetylation. *iScience* **21**, 773-788,
1024   doi:10.1016/j.isci.2019.10.053 (2019).

1025 55 Zhang, H., Roberts, D. N. & Cairns, B. R. Genome-wide dynamics of Htz1, a
1026   histone H2A variant that poises repressed/basal promoters for activation through
1027   histone loss. *Cell* **123**, 219-231, doi:10.1016/j.cell.2005.08.036 (2005).
1028 56 Van de Velde, S. *et al.* CREB Promotes Beta Cell Gene Expression by Targeting
1029   Its Coactivators to Tissue-Specific Enhancers. *Mol Cell Biol* **39**,
1030   doi:10.1128/MCB.00200-19 (2019).
1031 57 Choudhuri, A. *et al.* Common variants in signaling transcription-factor-binding sites
1032   drive phenotypic variability in red blood cell traits. *Nat Genet* **52**, 1333-1345,
1033   doi:10.1038/s41588-020-00738-2 (2020).
1034 58 Swinstead, E. E. *et al.* Steroid Receptors Reprogram FoxA1 Occupancy through
1035   Dynamic Chromatin Transitions. *Cell* **165**, 593-605, doi:10.1016/j.cell.2016.02.067
1036   (2016).
1037 59 Liu, Z. & Kraus, W. L. Catalytic-Independent Functions of PARP-1 Determine Sox2
1038   Pioneer Activity at Intractable Genomic Loci. *Mol Cell* **65**, 589-603 e589,
1039   doi:10.1016/j.molcel.2017.01.017 (2017).
1040 60 Donaghey, J. *et al.* Genetic determinants and epigenetic effects of pioneer-factor
1041   occupancy. *Nat Genet* **50**, 250-258, doi:10.1038/s41588-017-0034-3 (2018).
1042 61 de Pater, E. *et al.* Gata2 is required for HSC generation and survival. *J Exp Med*
1043   **210**, 2843-2850, doi:10.1084/jem.20130751 (2013).
1044 62 Wu, D. *et al.* Three-tiered role of the pioneer factor GATA2 in promoting androgen-
1045   dependent gene expression in prostate cancer. *Nucleic Acids Res* **42**, 3607-3622,
1046   doi:10.1093/nar/gkt1382 (2014).
1047 63 Sherwood, R. I. *et al.* Discovery of directional and nondirectional pioneer
1048   transcription factors by modeling DNase profile magnitude and shape. *Nat
1049   Biotechnol* **32**, 171-178, doi:10.1038/nbt.2798 (2014).
1050 64 Zhu, F. *et al.* The interaction landscape between transcription factors and the
1051   nucleosome. *Nature* **562**, 76-81, doi:10.1038/s41586-018-0549-5 (2018).
1052 65 Zaret, K. S. Pioneer Transcription Factors Initiating Gene Network Changes. *Annu
1053   Rev Genet* **54**, 367-385, doi:10.1146/annurev-genet-030220-015007 (2020).
1054 66 Dalvai, M., Fleury, L., Bellucci, L., Kocanova, S. & Bystricky, K. TIP48/Reptin and
1055   H2A.Z requirement for initiating chromatin remodeling in estrogen-activated
1056   transcription. *PLoS Genet* **9**, e1003387, doi:10.1371/journal.pgen.1003387
1057   (2013).
1058 67 Johnson, T. A. *et al.* Conventional and pioneer modes of glucocorticoid receptor
1059   interaction with enhancer chromatin in vivo. *Nucleic Acids Res* **46**, 203-214,
1060   doi:10.1093/nar/gkx1044 (2018).
1061 68 Valdes-Mora, F. *et al.* Acetylated histone variant H2A.Z is involved in the activation
1062   of neo-enhancers in prostate cancer. *Nat Commun* **8**, 1346, doi:10.1038/s41467-
1063   017-01393-8 (2017).
1064 69 Valdes-Mora, F. *et al.* Acetylation of H2A.Z is a key epigenetic modification
1065   associated with gene deregulation and epigenetic remodeling in cancer. *Genome
1066   Res* **22**, 307-321, doi:10.1101/gr.118919.110 (2012).
1067 70 Ishibashi, T. *et al.* Acetylation of vertebrate H2A.Z and its effect on the structure of
1068   the nucleosome. *Biochemistry* **48**, 5007-5017, doi:10.1021/bi900196c (2009).
1069 71 Yamagata, K., Shino, M., Aikawa, Y., Fujita, S. & Kitabayashi, I. Tip60 activates
1070   Hoxa9 and Meis1 expression through acetylation of H2A.Z, promoting MLL-AF10

and MLL-ENL acute myeloid leukemia. *Leukemia* **35**, 2840-2853, doi:10.1038/s41375-021-01244-y (2021).

72   Hottiger, M. O. & Nabel, G. J. Interaction of human immunodeficiency virus type 1 Tat with the transcriptional coactivators p300 and CREB binding protein. *J Virol* **72**, 8252-8256, doi:10.1128/JVI.72.10.8252-8256.1998 (1998).

73   Zhong, H., Voll, R. E. & Ghosh, S. Phosphorylation of NF-kappa B p65 by PKA stimulates transcriptional activity by promoting a novel bivalent interaction with the coactivator CBP/p300. *Mol Cell* **1**, 661-671, doi:10.1016/s1097-2765(00)80066-0 (1998).

74   Merika, M., Williams, A. J., Chen, G., Collins, T. & Thanos, D. Recruitment of CBP/p300 by the IFN beta enhanceosome is required for synergistic activation of transcription. *Mol Cell* **1**, 277-287, doi:10.1016/s1097-2765(00)80028-3 (1998).

75   Ravens, S., Yu, C., Ye, T., Stierle, M. & Tora, L. Tip60 complex binds to active Pol II promoters and a subset of enhancers and co-regulates the c-Myc network in mouse embryonic stem cells. *Epigenetics Chromatin* **8**, 45, doi:10.1186/s13072-015-0039-z (2015).

76   Santoriello, C. *et al.* RNA helicase DDX21 mediates nucleotide stress responses in neural crest and melanoma cells. *Nat Cell Biol* **22**, 372-379, doi:10.1038/s41556-020-0493-0 (2020).

77   Langmead, B. & Salzberg, S. L. Fast gapped-read alignment with Bowtie 2. *Nat Methods* **9**, 357-359, doi:10.1038/nmeth.1923 (2012).

78   Zhang, Y. *et al.* Model-based analysis of ChIP-Seq (MACS). *Genome Biol* **9**, R137, doi:10.1186/gb-2008-9-9-r137 (2008).

79   Ramirez, F. *et al.* deepTools2: a next generation web server for deep-sequencing data analysis. *Nucleic Acids Res* **44**, W160-165, doi:10.1093/nar/gkw257 (2016).

80   Kharchenko, P. V., Tolstorukov, M. Y. & Park, P. J. Design and analysis of ChIP-seq experiments for DNA-binding proteins. *Nat Biotechnol* **26**, 1351-1359, doi:10.1038/nbt.1508 (2008).

81   Lion, M., Muhire, B., Namiki, Y., Tolstorukov, M. Y. & Oettinger, M. A. Alterations in chromatin at antigen receptor loci define lineage progression during B lymphopoiesis. *Proc Natl Acad Sci U S A* **117**, 5453-5462, doi:10.1073/pnas.1914923117 (2020).